Journal of Nanobiotechnology

RESEARCH

Open Access

Platycodon grandiflorum exosome-like nanoparticles: the material basis of fresh platycodon grandiflorum optimality and its mechanism in regulating acute lung injury

Jingmin Fu[1†], Zhuolin Liu[2†], Zhiying Feng[1†], Jiawang Huang[2], Jianing Shi[1], Kangyu Wang[1], Xuelian Jiang[1], Jiaxin Yang[1], Yi Ning[3,4*], Fangguo Lu[3,4*] and Ling Li[2,4*]

Abstract

Background Acute lung injury (ALI) is a severe respiratory disease accompanied by diffuse inflammatory responses induced by various clinical causes. Many fresh medicinal plants have shown better efficacy than their dried forms in preventing and treating diseases like inflammation. As a classical Chinese herb, platycodon grandiflorum (PG) has been demonstrated effective in treating pneumonia, but most of previous studies focused on the efficacy of processed or dried PG formats, while the specific benefits of its fresh form are still underexplored. Exosome-like nanoparticles derived from medicinal plants are expected to point out an important direction for exploring the material basis and mechanism of this fresh herbal medicine.

Results The fresh form of PG could effectively improve ALI induced by lipopolysaccharide (LPS), relieve lung histopathological injury and weight loss, and reduce levels of inflammatory factors in mice, exhibiting better efficacy than dried PG in the treatment of ALI. Further extraction and purification of PG exosome-like nanoparticles (PGLNs) demonstrated that PGLNs had good biocompatibility, with characteristics consistent with general exosome-like nanoparticles. Besides, proteomic analysis indicated that PGLNs were rich in a variety of proteins. Animal experiments showed that PGLNs improved the pathological changes in LPS-induced lung tissues, inhibited the expression of inflammatory factors and promoted the expression of anti-inflammatory factors, and exerted a regulatory effect on the polarization of lung macrophages. Cell experiments further confirmed that PGLNs could be effectively taken up by RAW264.7 cells and repolarize M1 macrophages into M2 type, therefore reducing the secretion of harmful cytokines. Moreover, non-targeted metabolomics analysis reveals that PGLNs reduce inflammation and

†Jingmin Fu, Zhuolin Liu and Zhiying Feng contributed equally to this work and share first authorship.

*Correspondence:
Yi Ning
004217@hnucm.edu.cn
Fangguo Lu
001196@hnucm.edu.cn
Ling Li
liling1049@hnucm.edu.cn

Full list of author information is available at the end of the article

control macrophage polarization in a manner closely linked to pathways including glycolysis and lipid metabolism, highlighting a potential mechanism by which PGLNs protect the lungs from inflammatory damage like ALI.

Conclusion Fresh PG has better anti-inflammatory and repair effects than its dried form. As one of the most effective active substances in fresh PG, PGLNs may regulate macrophage inflammation and polarization by regulating metabolic pathways including lipid metabolism and glycolysis, so as to reduce inflammation and repair lung injury.

Graphical Abstract

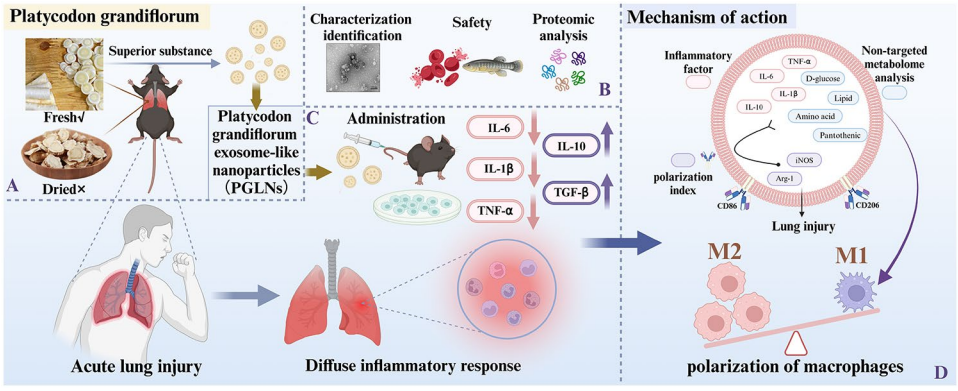

Keywords Platycodon grandiflorum, PGLNs, Fresh medicinal plant, Macrophage polarization, Acute lung injury, Non-targeted metabolomics

Introduction

Acute lung injury (ALI) is an acute inflammatory lung injury of the alveolar epithelium and interstitium induced by a range of causes, characterized by inflammatory cell infiltration, increased permeability of the alveolar capillary barrier and acute diffuse alveolar edema. It is a life-threatening hypoxic respiratory disease with a mortality rate of up to 40% [1]. At present, there is no effective clinical treatment to improve the survival rate of ALI worldwide, and patients can only receive supportive treatment. Most of the existing medications are corticosteroid drugs, which often produce serious adverse reactions [2].

Non-processed fresh Chinese herbs not only present the initial form of herbal medicine, but also reflect a major feature of traditional Chinese medicine as a treasure of Chinese culture. Fresh herbs have long been used in clinical practice, showing stronger medicinal efficacy and therapeutic effects than dried herbs in a variety of diseases [3, 4]. Platycodon grandiflorum (PG), as a classical Chinese herbal medicine, has a profound history in treating respiratory infections, bronchitis, pneumonia, and other lung-related diseases. According to previous reports, PG possesses anti-inflammatory, anticancer, antiviral, immunomodulatory and hypoglycemic pharmacological properties [5, 6].

In recent years, the application of nanotechnology in biomedicine has been drawing growing attention worldwide. Nanomedicine carriers are characterized by multiple advantages, such as small size, large specific surface area, controlled matrix release, and targeted drug delivery [7], for which extensive studies have explored their potential applications for achieving targeted drug delivery in anti-inflammatory, antibacterial and other aspects [8–10]. However, some inorganic compounds and nanoparticles generated by certain organic compounds cannot be cleared by human metabolism, and may accumulate in the body to cause toxicity, such as teratogenicity and sensitization [11, 12], which need to be properly addressed.

Tiny but powerful exosomes, while reshaping the paradigm of medical research, have also led the forefront of the development of biology. Nowadays, plant exosome-like nanoparticles, a kind of nanoscale membrane vesicles actively released by plant cells, have attracted a great interest in the global academic context. Plant exosome-like nanoparticles play important roles in information and material transfer in intercellular and interspecies communication [13]. Such nanoparticles from medicinal plants, especially from Chineseherbs, naturally incorporate homologous bioactive constituents with pharmacodynamic properties, which exert a natural multi-component synergistic effect that greatly improves the bioavailability of some traditional Chinese medicine monomers, therefore manifesting unique activity and efficacy [14]. Studies have shown that exosome-like nanoparticles extracted from ginseng, ginger, dandelion and pueraria can alleviate inflammation, inhibit tumor proliferation and prevent high blood pressure [15–17].

However, whether exosome-like nanoparticles derived from medicinal plants are a major reason for the better efficacy of fresh herbs has not been fully clarified.

In this context, we first examined the therapeutic effects of fresh PG on ALI mice. Then, we obtained PG exosome-like nanoparticles (PGLNs) for the first time using differential centrifugation and the sucrose density gradient method, and characterized their physicochemical properties and chemical composition by electron microscopy, particle size, Zeta potential, agar-gel electrophoresis, SDS-PAGE, and proteomic analysis. Meanwhile, we evaluated the biosafety and biocompatibility of PGLNs, and further investigated their therapeutic potential to repair inflammatory injury based on in vivo and in vitro experiments. Subsequently, whether this unique bioactive substance is an important medium for fresh PG to exert its anti-ALI efficacy and what the specific mechanism is were explored from the perspective of macrophage polarization combined with metabolomics analysis. We believe that combining fresh Chinese herbs with the emerging technology of exosome-like nanoparticles may be a green, safe and effective solution for treating a variety of diseases, including ALI, and has good research and application prospects in terms of biological activity, drug delivery routes, and dosage form development.

Materials and methods

Animals and cells

The C57BL/6J male mice (6–8 weeks old, 18–22 g) were purchased from Hunan Lake Jingda Laboratory Animal Co., Ltd. (quality certificate No.430727231102973863), and were kept in the Animal Experiment Center of Hunan University of Chinese Medicine. The wild-type AB Zebrafish were obtained from the National Zebrafish Resource Center and maintained in the Zebrafish breeding system of Hunan Key Laboratory of Hunan University of Chinese Medicine (Beijing Aiseng Technology Development Co., Ltd.). The zebrafish were placed in an environment of 28 ± 1℃ with a 14-hour light / 10-hour dark cycle (photocycle from 7 am to 10 PM), and adult fish aged 90–290 days were selected for the experiments. Natural mating was employed to breed zebrafish larvae, and fish embryos 1 day after fertilization were used for formal analyses. All animal experiments were approved by the Ethics Committee of the Center for Animal Experiments of Hunan University of Chinese Medicine (Approval number: SLBH-202307190001). The mouse mononuclear macrophages cell line (RAW264.7) was obtained from the Chinese Academy of Sciences Cell Bank.

Reagents

The DMEM basic culture solution (lot number: WH0021D031), phosphate buffer (PBS) (lot number: WH0021D081), serum-free non-programmed frozen solution (lot number: WH0021A081), and double antibody (penicillin, streptolycin, lot number: WH1021A161) were all purchased from Wuhan Penocai Life Technology Co., Ltd. The fetal bovine serum (lot number: SA210518) was purchased from Thermo Fisher Technology Co., Ltd. The cell-specific lipopolysaccharides (LPS-L2630, lot number: 0000155608) and animal-specific lipopolysaccharides (LPS-L2800, lot number: 0000189843) were purchased from Sigma-Aldrich. The CCK8 cell proliferation-toxicity detection kit (lot number: BS350A) was purchased from Biosharp. The BCA protein quantitative kit (batch number: 81910335A) was purchased from Lianke Biotechnology Co., Ltd. The mRNA reverse transcription primers and real-time quantitative polymerase chain reaction (RT-qPCR) primers were synthesized by Shenggong BioEngineering (Shanghai) Co., Ltd. The CD86 antibodies (lot number: 13395-1-AP) and CD206 antibodies (lot number: 18704-1-AP) were purchased from Proteintech. The 4',6-diamidino-2-phenylindole (4',6-Diamidino-2-phenylindole, DAPI) solution, rhodamine phalloidin, and tetramethyl isothiocyanate (TRITC) were purchased from Beijing Soleibaol Technology Co., Ltd. The fluorescein isothiocyanate isomer (FITC) was purchased from Proteintech. Anti-CD11b-FITC(lot number: 4012900) and anti-CD86-PE-Cy7(lot number: 4221282) was purchased from BD Pharmingen™, USA, Anti-F4/80-BV421(lot number: 2920767) and anti-CD206-PE(lot number: 2535977) was purchased fromInvitrogen, USA.

Instruments

The experimental instruments used in this study include: table top high speed refrigerated centrifuge (Thermo, USA), ELX800-enzyme spectrometer (Bio-tek, ELX800, USA), optima MAX-XP table top ultra-centrifuge, ultrafiltration tube (Merck millipore, Amicon Ultra-15, Ultracel-30 K), concentrated tube (Beckman, Centrifuge Tubes), Nanoparticle Tracking analyzer (Malvern Panalytical, Zetasizer Pro), Nanoparticle size potentiometric analyzer (Malvern Panalytical, ZetaView), CO_2 cell incubator (Thermo Fisher Scientific), inverted microscope (Motic), ultra-high resolution laser confocal microscope (Zeiss), real-time quantitative PCR instrument (BioTek), chemiluminescence imager and synergy2 multifunctional enzyme label (BioTek), transmission electron microscopy (Hitachi (China) Co., Ltd.), micropipette (Poland High Tech Lab), electric thermostatic water bath (Shanghai Jinghong Experimental Equipment Company), ultramicrospectrophotometer (Bole Life Medical Products (Shanghai) Co., Ltd.), and SY-5000 rotary evaporation instrument (Shanghai Yarong Biochemical Instrument Factory), the BD FACSCanto™ flow cytometer(BD biosciences, USA).

Preparation of fresh liquid extract and distilled liquid from PG

Fresh PG roots (sourced from Chifeng, Inner Mongolia, China) were washed with deionized water, cut into small pieces, and fully ground at low temperature with appropriate amount of pre-cooling PBS in a slow juicer to obtain fresh PG juice. The juice was centrifuged at 4 ℃, 2000×g for 20 min. After discarding residues, the supernatant was collected, placed in a round bottom flask, and concentrated using a rotary evaporator. The concentrated fresh liquid extract (PF) and distilled liquid (PFW) of PG were collected respectively and stored at -40 ℃.

Preparation of dried PG, dried PG extract, and distilled liquid from dried PG

The fresh PG slices were pre-frozen in a -80 ℃ refrigerator, then placed in a vacuum freeze dryer overnight, and freeze-dried at -40 ℃, 110KPa for 48 h. The dried products were measured to calculate the drying rate. Subsequently, the dried product was pulverized into powder using a grinder, extracted twice with ten times distilled water, and concentrated through a rotary evaporator. After concentration, the dried PG extract (PD) and distill liquid from dried PG (PDW) were collected respectively and stored at -40 ℃.

Preparation of PGLNs

The fresh PG juice was centrifuged at 4 °C, 500×g for 10 min, 2000×g for 20 min, and finally 10,000×g for 30 min to remove large particles and fibers. The final supernatant was filtered with a 0.45 μm microporous filter membrane and centrifuged at 4 ℃, 120,000×g ultra-fast for 60 min. The obtained crude extraction precipitate was re-suspended in PBS and centrifuged with the sucrose density gradient (8%, 30%, 45% and 60%) at 4 ℃, 120,000×g for 90 min. The bands of 8-30% sucrose layer and 30-45% sucrose layer were collected and washed properly. Finally, purified PGLNs were obtained and re-suspended in sterile PBS (to be used as fresh or store at -80 ℃).

Characterization and identification of PGLNs

Electron microscope observation

The obtained PGLNs were absorbed by capillary tubes and dropped onto a copper mesh with a supporting film. After resting still for 3–5 min, the copper mesh was removed, and the remaining water droplets were absorbed. After the excess water content was completely evaporated, a small drop of 3% phosphotungstic acid solution was added on the wax dish. The copper mesh containing the sample was gently put onto the surface of the dye solution, allowing the sample to tightly contact with the dye solution and stand still for 3–5 min. Then, the copper mesh was removed, and the excess liquid droplets were absorbed again. After natural drying, electron microscope images were taken and observed.

Nanoparticle tracking analysis and zeta potential analysis

The obtained PGLNs were added to 1mL PBS for re-suspension and mixing. Then, 0.2mL suspension was added to the colorimetric dish. The experimental data were analyzed by Origin2021 software using the BT-Zeta100 nanometer particle size and Zeta potential analyzer.

Coomassie brilliant blue staining

The protein of PGLNs was extracted with RIPA lysate, and was subjected to electrophoresis with 4×SDS polyacrylamide gel after denaturation. Subsequently, 10% SDS-PAGE was cut off and subjected to Coomassie blue staining for 2 h, and then rinsed with bleaching solution for 2–3 times, 1–2 h each (bleaching solution: 95% ethanol 2,250 mL + glacial acetic acid 250 mL + distilled water 2,500 mL). The protein in the supernatant was analyzed using a gel imaging analysis system.

Detection of PGLNs concentration by BCA

The obtained PGLNs were added to 1mL PBS for re-suspension. According to the instructions of the BCA kit, 20 μL suspension was added into each well of a 96-well plate, with 3 wells for each group. Then, BCA working fluid was added, and the plate was incubated in an oven at 37℃ for 30 min. The absorbance value (OD value) was detected at 562 nm wavelength, and the concentration of PGLNs was calculated.

Gel electrophoresis of agarose

The prepared agarose gel was poured into the electrophoresis tank and allowed to solidify at room temperature for 30 minutes. A mixture of 5 μL RNA sample, 1 μL loading buffer, and 1 μL nucleic acid dye was prepared and thoroughly mixed, then loaded into the sample wells. The gel was placed in the electrophoresis chamber, submerged in 1× TAE buffer, and electrophoresed at 120 V for 60 minutes. Following electrophoresis, RNA bands were visualized and documented using a UV gel imaging system.

Proteomics of PGLNs

GLNs proteins were lysed with 2% sodium deoxycholate, followed by ultrasonic treatment, denaturation at 95 °C, centrifugation, and collection of the supernatant for quantification and aliquoting. Protein concentration was determined using the Bradford method, and SDS-PAGE was used to verify the integrity of the proteins. A total of 50 μg of protein was digested with Trypsin (37 °C,16 h), desalted using a Waters solid-phase column, and stored frozen. Mass spectrometry was performed using the Thermo EASY-nLC1200 system equipped with a homemade C18 column (100 μm × 35 cm,1.8 μm) for gradient

elution (4%–90% acetonitrile/0.1% formic acid). Data were acquired in DDA mode on an Orbitrap Exploris480 mass spectrometer with a resolution of 60,000 for MS1 and 15,000 for MS2. Database searching was conducted using MaxQuant software (v2.1.4.0) against the UniProt database, with settings for trypsin digestion, cysteine alkylation as fixed modifications, and methionine oxidation as variable modifications, with a false discovery rate (FDR) <1%. Differentially expressed proteins were identified with criteria of |FC| >1.2 and P <0.05. GO/KEGG pathway enrichment analysis was performed using the metaX package in R, and subcellular localization was predicted using WoLF PSORT.

Evaluation of biocompatibility of PGLNs

Zebrafish experiment

Two male and one female zebrafish were placed in a breeding tank overnight in a dark environment. Lights were turned on the next morning and the dividers were removed, leaving the fish free to lay eggs and fertilize. To minimize genetic variation, the fish eggs were collected and randomly assigned to at least three groups. The fertilized eggs were then placed in 6-well plates and divided into 6 groups, with PGLNs concentrations of 1, 5, 10, 50, and 100 μg/mL, respectively, alongside a normal control group. The eggs were kept at 28 ± 2 °C for 96 h after fertilization, and the teratogenic and lethal effects on juvenile fish were observed.

Hemolysis test

The fresh whole blood of chicken was collected in a BD tube containing anticoagulant. The tube was thoroughly shaken to well mix the blood with the anticoagulant, and was then centrifuged at 3000 rpm for 15 min. After removing the supernatant, the red blood cell precipitation was suspended with PBS/ normal saline, centrifuged under the same conditions, and washed for 3–4 times until the supernatant was clarified. Subsequently, the erythrocyte suspension was prepared with PBS/ normal saline and 2-4% erythrocyte suspension, and was temporarily stored in the refrigerator at 4 ℃ for later use. A positive control group (pure water) and a negative control group (PBS), as well as 6 PGLNs groups with concentrations of 0, 10, 50, 100, 500 and 1000 μg/mL were set up. Further, 500 uL red blood cell suspension was added into EP tubes, which were supplemented with the same volume of pure water, PBS, and different concentrations of PGLNs, respectively. After incubation at 37℃ for 1 h, the tubes were subjected to centrifugation at 2400 rpm for 5 min, and the supernatant was taken to measure the OD value at 540 nm. Lastly, the hemolysis rate was determined based on the following equation: hemolysis rate = (OD sample test group - OD negative control group) ÷ (OD positive control group - OD negative control group) × 100%. For the concentration of 1000 μg/mL, the hemolysis rate of PGLNs was less than 20%, showing a low hemolysis activity.

CCK8

RAW264.7 cells were added in a 96-well plate (4×10^3 cells/well). After 24 h of culture, the cells were mixed with PGLNs at the concentrations of 0, 0.5, 1, 5, 10, 25, 50, 100, 250 μg/mL, respectively, and were incubated for 24 h. Then, the absorbance value was determined at 450 nm wavelength according to the operating instructions of the cell proliferation and virus detection kit: cell relative viability rate (%) = (experimental group A mean ÷ control group A mean) × 100%.

Toxic effects of PGLNs on mouse organs observed by H&E staining

After one week of adaptive feeding, 6 SPF male C57BL/6J mice, weighing 18–22 g, were randomly divided into the normal control group (Con) and PGLNs group (PGLNs). After resting for 6 h, the liver, heart, spleen, lung and kidney tissues were sampled and fixed with 4% paraformaldehyde, dehydrated with ethanol gradient, treated for transparency with xylene, impregnated with wax, and embedded with paraffin. Then, discontinuous 5 μm-thick sections were sliced, stained with HE, dehydrated, treated for transparency, and sealed properly. The toxic effects were observed under a microscope.

Treatment of ALI model mice by PF, PD, PFW and PDW

After one week of adaptive feeding, 24 SPF male C57BL/6J mice, weighing 18–22 g, were randomly divided into the Con group, LPS group, LPS + PF group, LPS + PD group, LPS + PFW group and LPS + PDW group, with 4 mice in each group. The Con and LPS groups were treated with pure water, while the other groups were treated with PF, PD, PFW and PDW, respectively, for 7 days (Dosage: PD 1 g/kg, PF 10 g/3 kg, 100 μL/day). Then, the mice in each group except for the Con group were given 5 mg/kg LPS for intratracheal instillation modeling, and the Con group was given the same amount of PBS [18]. After 24 h of modeling, the alveolar lavage fluid and organ tissues were separated for further testing. Throughout the entire experimental process, the general indicators of the mice including activity, hair color, diet, and weight were monitored and recorded daily.

PGLNs treatment on ALI model mice

After one week of adaptive feeding, 18 SPF grade male C57BL/6J mice, weighing 18–22 g, were randomly selected and assigned to the Con group. The remaining mice were first given 5 mg/kg LPS for endotracheal injection modeling, and then randomly divided into the

LPS group and LPS + PGLNs group. After 6 h of modeling, the mice in the LPS + PGLNs group were injected with 5 mg/kg PGLNs via tail vein, while the Con group and LPS group were injected with equal amounts of PBS [19]. After 24 h of administration, the alveolar lavage fluid and organ tissues were separated for further testing. Throughout the entire experimental process, the general indicators of the mice including activity, hair color, diet, and weight were monitored and recorded daily.

Detection of protein content in alveolar lavage fluid by BCA

The obtained alveolar lavage liquid of each group was added to 1 mLPBS for re-suspension. According to the instructions of the BCA kit, 20 μL suspension was added to each well of a 96-well plate, with 3 wells for each group. Then, BCA working fluid was added, and the plate was incubated in an oven at 37 ℃ for 30 min. Subsequently, the OD value was detected at 562 nm wavelength, and the functional exosome concentration was calculated for each group.

Detection of mRNA expression in mouse lung tissues by RT-qPCR

The total RNA was extracted from mouse lung tissues by the Trizol method, and 1 μg RNA was reversely transcribed into cDNA according to instructions of the reverse transcription kit, which was amplified by the fluorescence quantitative PCR kit. The qPCR reaction conditions were set as follows: predenaturation at 95 ℃ for 30 s, denaturation at 95 ℃ for 10 s, and annealing and extension at 60 ℃ for 30 s, for 40 cycles. The relative expression of related genes was calculated by the $2^{-\Delta\Delta Ct}$ method with β-actin as the internal reference. The primer sequences were shown in Table 1.

Table 1 Primer sequences in RT-qPCR

Name	Primer sequence(5′→3′)
TNF-*α*-F	GGTGTTGCCTGCTGCCTTCC
TNF-*α*-R	GTTCTGAAGAGGTGAGTGGCTGTC
IL-6-F	CTGGCGGAGGAGGTGCTCTC
IL-6-R	GGAGGAAGGAGAAGAGGCTGAGG
IL-1*β*-F	GGTGTTGCCTGCTGCCTTCC
IL-1*β*-R	GTTCTGAAGAGGTGAGTGGCTGTC
IL-10-F	AGAGAAGCATGGCCCAGAAATCAAG
IL-10-R	CTTCACCTGCTCCACTGCCTTG
TGF*β*1-F	GGCTACTGCCGCTTCTGCTC
TGF*β*1-R	CCAGCTCCATGTCGATGGTCTTG
Arg-1-F	TGTCCCTAATGACAGCTCCTT
Arg-1-R	GCATCCACCCAAATGACACAT
iNOS-F	ATCTTGGAGCGAGTTGTGGATTGTC
iNOS-R	TAGGTGAGGGCTTGGCTGAGTG
β-actin-F	ACGCCAACACAGTGCTGTCTG
β-actin-R	TGCTTGCTGATCCACATCTGCTG

Observation of histopathological changes by H&E staining

Mouse lung tissues were extracted and subjected to HE staining following the previous procedure. Then, the histopathological changes of mice in each group were observed.

Cell experiment

Cell culture

RAW264.7 macrophages were cultured with 10% fetal bovine serum, 1% double antibody and 90% basic culture medium in a 5% CO_2 incubator at 37℃, with the cell culture medium replaced on a daily basis. When the cells grew to 90%, 0.25% trypsin was used for digestion and passage.

CCK8

RAW264.7 cells were added into a 96-well plate (4×10^3 cells/well). After 24 h of culture, the cells were mixed with LPS at the concentrations of 0, 1, 5, 10, 15, 20, 25, 30 μg/mL, respectively, and were incubated for 24 h. Then, the absorbance value was determined at 450 nm wavelength according to the operating instructions of the cell proliferation and virus detection kit: cell relative inhibition rate (%) = (1- experimental group A mean ÷ control group A mean) × 100%.

Construction of acute cell injury model and intervention with PGLNs

RAW264.7 macrophages were divided into the Con group, LPS group and LPS + PGLNs group. The macrophages in each group were inoculated in 6-well plates at the density of 1×10^6 cells/well and cultured for 24 h. Then, the LPS group and LPS + PGLNs group were added with 1 μg/mL LPS, while the LPS + PGLNs group was added with both 1 μg/mL LPS and 20 μg/mL PGLNs for intervention for 24 h.

Detection of mRNA expression in cells by RT-qPCR

Same as the procedure in animal experiment. The primer sequences were shown in Table 1.

Immunofluorescence

RAW264.7 cells were divided into 3 groups (Con group, LPS group, and LPS + PGLNs group), and were inoculated in 6-well plates paved with climbing plates, with 2 mL of complete culture solution in each well, in a constant temperature (37 ℃) incubator for 12 h. The PGLNs were incubated with PKH67 dye at room temperature for 2 h for fluorescence labeling. The waste liquid in the plates was discarded. Then, the LPS group was added with LPS and the LPS + PGLNs group was added with both LPS and PGLNs, and were incubated at 37 ℃ for 24 h. Subsequently, the cell crawling tablets were collected and soaked with PBS twice (3 min each) for the

following operations: (1) fix with 4% paraformaldehyde for 15 min, and soak with PBS 3 times (3 min each); (2) permeate with 0.5% TritonX-100 at room temperature for 20 min, and soak with PBS 3 times (3 min each); (3) fully absorb the PBS, drip with rhodamine, incubate at room temperature for 20 min away from light, and soak with PBS 5 times (3 min each); (4) fully absorb the PBS, drip with DAPI, incubate at room temperature for 5 min away from light, and soak with PBS 8 times (3 min each). The anti-fluorescence quench agent was added to the tablets, which were inverted onto the slide to observe under a fluorescence microscope.

Flow cytometry

Construction of acute cell injury model and intervention with PGLNs is the same as in other cell experiments. To detect CD11b, F4/80 macrophages, anti-CD11b-FITC, anti-F4/80-BV421, anti-CD86-PE-Cy7 and anti-CD206-PE were used to stain cells. Isotype controls were run in parallel. Flow cytometry was performed using the BD FACSCanto™ flow cytometer.

Metabolomics

Macrophages were collected from each group, and were added with an appropriate volume of extraction solution and magnetic beads for grinding and ultrasonic treatment. The supernatant was taken for vacuum drying after static centrifugation, and was then added with an appropriate amount of extraction solution for redissolution and machine testing. Chromatographic separation was performed on Waters ACQUITY UPLC HSS T3 column (2.1 mm × 100 mm, 1.8 μm) at 45 ℃ using 0.1% formic acid aqueous solution (A) or methanol (B) as the mobile phase (flow rate: 0.35 mL/min, injection volume: 10 μL). The following gradient procedure was adopted as elution conditions: 0–1.5 min, 95%A; 1.5–3 min, 95%-70%A; 3–5 min, 70%-40%A; 5–7 min, 40%-20%A; 7–12 min, 20%-0 A; 12–16 min, 0 A; 16–18.5 min, 0–95%A. The mass spectrum conditions were set as follows: range, 60–900 Da; full scanning resolution, 70,000; ddMS2 mass resolution, 17,500; flow rate of sheathing gas, 30 Arb; capillary temperature, 320 ℃. The mass spectrum data were collected in both positive ionization (ESI+) and negative ionization (ESI-) modes (spray voltage: positive, 3,500 V; negative, 3,100 V). The metabolites were identified using OSI/SMMS software (Dalian Institute of Chemical Physics, Chinese Academy of Sciences, Dalian Chemical Data Information Technology Co., Ltd.) according to the results of comparison between precursor ions and secondary fragments. Standard databases including Human Metabolome Database (HMDB, https://hmdb.ca/) and metabolite database (METLIN, http://metlin.scripps.Edu) were referred to as the source database. The positive and negative ion data were merged into a data matrix and imported into the SIMCA platform for partial least square discriminant analysis (PLS-DA) and orthogonal partial least square discriminant analysis (OPLS-DA). Differential metabolites were screened based on the criteria of $|\log_2 FC| > 1$ and $P < 0.05$. Then, the biomarkers were further screened by combining the standard databases with the HMDB database, and the MetoboAnalysis6.0 (https://www.metaboanalyst.ca) database was used for pathway analysis.

Statistical analysis

The measurement data were tested to conform to normal distribution and homogeneity of variance, and were expressed as mean ± SD. One-Way ANOVA was used for comparisons among multiple groups. $P < 0.05$ was considered statistically significant. Statistical significance was defined as follows: $^{***}P<0.01$, $^{**}P<0.05$; $^{\#\#\#}P<0.01$, $^{\#\#}P<0.05$.

Results

PG improves LPS-induced lung pathological injury in mice

PG, as both a traditional Chinese herbal medicine and food ingredient, has been shown to possess anti-inflammatory, anticancer, antiviral, immunomodulatory and hypoglycemic properties, and is often used to treat respiratory tract infection, bronchitis, pneumonia and other lung-related diseases. In this study, we investigated the differences in lung anti-inflammatory effects between fresh and dried PG using a mouse model of LPS-induced ALI, and the experimental procedures are shown in Fig. 1A. Consistent with the expected results, the mice exhibited significant weight loss after LPS intervention, and histological results indicated that LPS stimulation caused alveolar wall thickening, pulmonary interstitial edema, alveolar hemorrhage, alveolar cavity collapse, and significant inflammatory cell infiltration in the alveolar cavity and pulmonary interstitial, suggesting extensive structural disorders in lung tissues. Treatment with fresh PG (PF) significantly recovered the general condition and pathological changes of lung tissues in mice, mainly manifested as alleviation in weight loss and improvement in lung tissue structure and inflammatory cell infiltration. In the dried PG (PD) group, weight loss and lung tissue inflammatory injury were also improved to a certain extent, but alveolar hemorrhage, interstitial edema, inflammatory cell infiltration and local alveolar wall thickening were still visible on histological examination (Fig. 1B, E). Meanwhile, both PF and PD treatments significantly reduced the total protein in the alveolar lavage fluid of mice with LPS-induced ALI, suggesting that PG, either fresh or dried, can effectively alleviate inflammatory exudation (Fig. 1C). Consistently, both PF and PD significantly reduced the mRNA expression of lung pro-inflammatory factors IL-1β, IL-6, and TNF-α in LPS-induced mice (Fig. 1D). In summary, these results

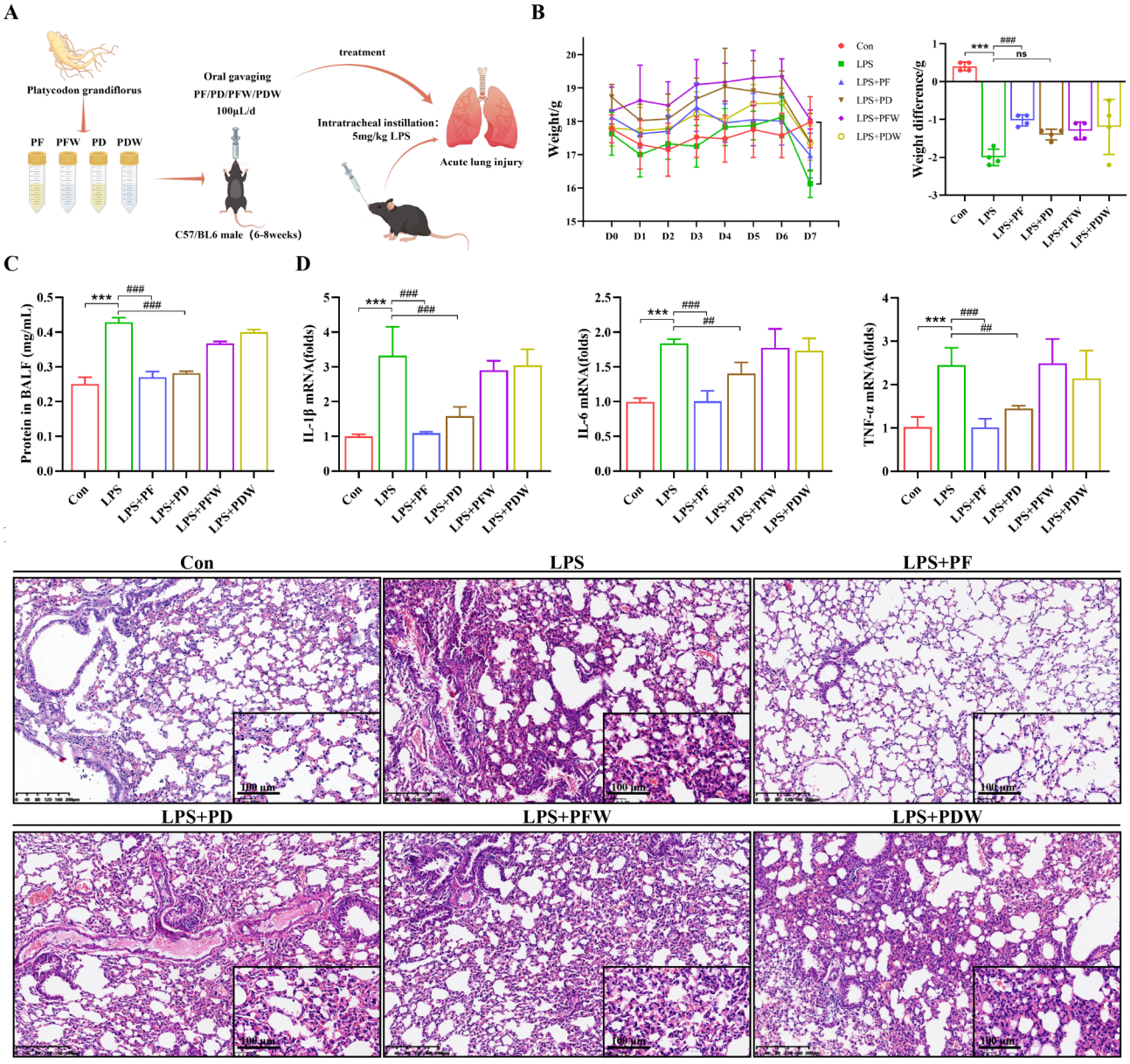

Fig. 1 Fresh PG shows a better therapeutic effect than dried PG in alleviating LPS-induced ALI in mice. (A) Administration of LPS and PG(PF, PFW, PD, PDW) in ALI model mice. (B) Weight changes in each group within 7 days after treatment with PF, PFW, PD and PDW, respectively (n =4). (C) Protein concentration in the alveolar lavage fluid of mice in each group (n = 4). (D) mRNA levels of IL-1β, IL-6 and TNF-α in mouse lung tissues in each group (n = 4). (E) H&E staining results of mouse lung sections in each group. Scale: 200μm and 100μm

indicate that intervention with fresh or dried PG can significantly repair lung inflammatory injury and improve lung pathological changes after LPS stimulation, with fresh PG showing a better therapeutic effect.

Isolation and characterization of PGLNs

The combination of ultrafine differential centrifugation and sucrose density gradient centrifugation is the current gold standard for extracting and purifying exosome-like nanoparticles from plant origins. In this study, PGLNs were extracted and purified by applying different relative centrifugal forces (RCF: 500-120,000) and sucrose density gradient solutions (8–60% w/v) (see the extraction process in Fig. 2A).

The morphology, zeta potential, particle size, and composition of PGLNs were analyzed and characterized using transmission electron microscopy (TEM), dynamic light scattering, nanoparticle tracking analyzer (NTA), agarose gel electrophoresis and SDS-PAGE electrophoresis, respectively. TEM observations showed that the PGLNs extracted manifested as circular or elliptical vesicles with a bilayer membrane structure with an

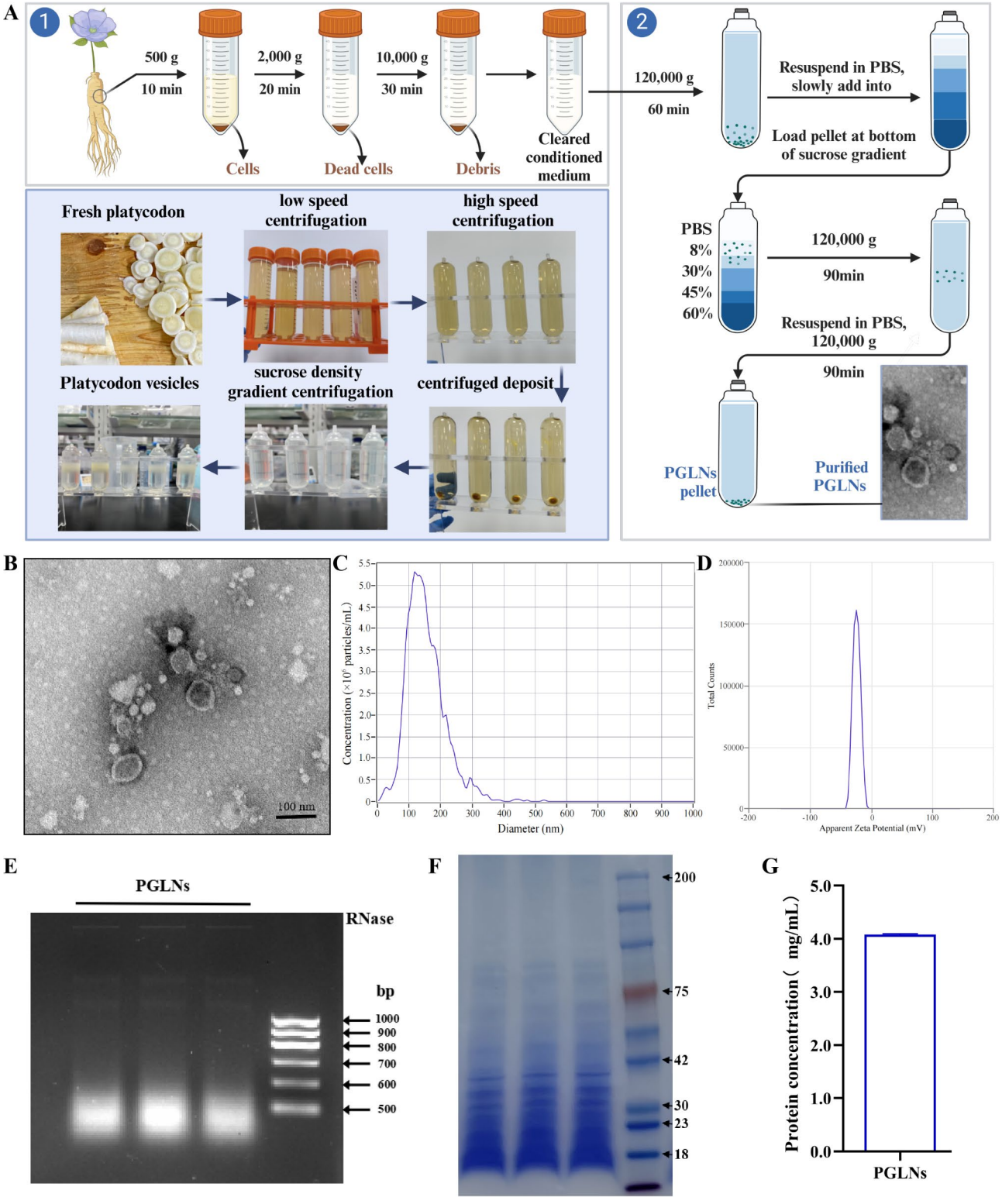

Fig. 2 Isolation and characterization of PGLNs. (A) Differential centrifugation and sucrose density gradient centrifugation for PGLNs preparation. (B) Transmission electron microscope (TEM) images of PGLNs. Scale, 100 nm. (C) Nanoparticle tracking analysis (NTA) to detect the size and particle number of isolated PGLNs. (D) The surface charge of PGLNs. (E) The nucleic acid content of PGLNs detected by agarose gel electrophoresis. The standard DNA molecular weight is used as a size marker. (F) The protein contents of PGLNs detected by SDS-PAGE (10%) and Coomassie brilliant blue staining. (G) The protein concentration of isolated PGLNs. The standard protein molecular weight is used as a molecular weight (MW) marker

average diameter of 90 nm (Fig. 2B), conforming to the general characteristics of exosome-like nanoparticles. NTA results showed that the average size distribution of PGLNs was 141.2 nm, with a high particle content (an average of 1.4×10^8 particles/mL) (Fig. 2C). The difference in the mean particle size of PGLNs measured by TEM and NTA can be attributed to the fact that PGLNs had been completely dehydrated at the time of TEM, but were in a swollen state at the time of NTA. The Zeta potential measurement results showed that the zeta potential of PGLNs is -23.5 mV (Fig. 2D), indicating good stability and dispersion. In addition, we analyzed the composition of PGLNs and detected the presence of nucleic acid and protein-related substances by agarose gel electrophoresis and SDS-PAGE electrophoresis, respectively (Fig. 2E, F). In order to quantify PGLNs, we measured the protein concentration of PGLNs using a BCA protein assay kit. The results showed that the concentration of fresh PGLNs was about 4.0 mg/mL, and 1mL PGLNs could be obtained from every 50 g of fresh PG, indicating a high yield rate (Fig. 2G). Subsequently, we conducted further proteomic analysis of PGLNs, and found that PGLNs contained a variety of peptides and proteins. Specifically, a total of 112 protein components were detected (Fig. 3A), of which about 70% of the proteins had a molecular weight of 0–80 kDa, and about 30% had a molecular weight greater than 80 kDa (Fig. 3B). The results of protein subcellular localization showed that 37 proteins were located in the cytoplasm and 15 proteins were located in the plasma membrane (Fig. 3C). GO and KEGG analyses revealed that PGLNs contained a variety of proteins related to membrane components, which were involved in signal transduction and various metabolic pathways. This further highlights the vesicle-like characteristics of PGLNs and their possible pharmacodynamic material basis.

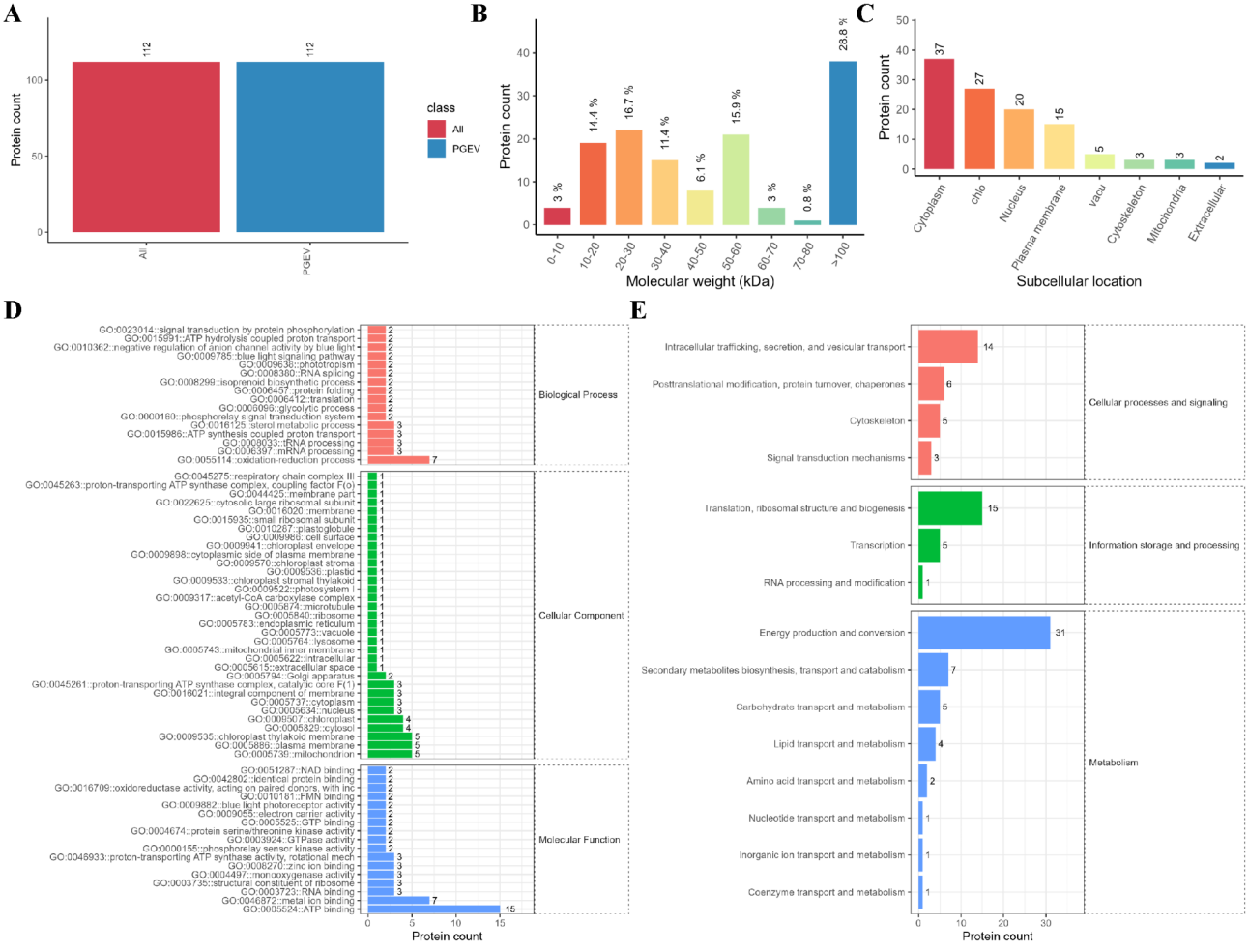

Fig. 3 Characterization of PGLNs - proteomics. Histogram shows (**A**) the total protein quantity, (**B**) the total protein molecular weight distribution, and (**C**) the total protein subcellular location identified in PGLNs. (**D**) GO function analysis results based on PGLNs proteomics. (**E**) KEGG analysis results based on PGLNs proteomics

PGLNs shows good biocompatibility

In order to further evaluate the biocompatibility of PGLNs and provide safety evidence for the subsequent animal experiment, toxicological tests were conducted from multiple biological levels, including blood entry, macrophages, zebrafish embryos and mouse tissues and organs. Firstly, hemolysis tests on red blood cells with different concentrations of PGLNs (1000, 500, 100, 50, 10 μg/mL) showed that all concentrations of PGLNs had low hemolysis activity (Fig. 4A), providing a basis for the intravenous administration of PGLNs. The results of cytotoxicity tests showed that the activity of RAW264.7 cells increased after 24 h of intervention with all concentrations of PGLNs, indicating that PGLNs can promote the proliferation of RAW264.7 cells (Fig. 4B). In order to examine the biocompatibility of PGLNs in vivo, 1 mg/mL of PGLNs was injected into the mice through tail vein, and samples were collected for H&E staining. The results showed that there were no obvious pathological changes in the morphology of liver, heart, spleen, lung and kidney tissues in the PGLNs group compared to the Con group, indicating good biosafety of PGLNs (Fig. 4C). Moreover, we evaluated the potential toxicity of PGLNs to zebrafish embryos by administering PGLNs at the concentrations

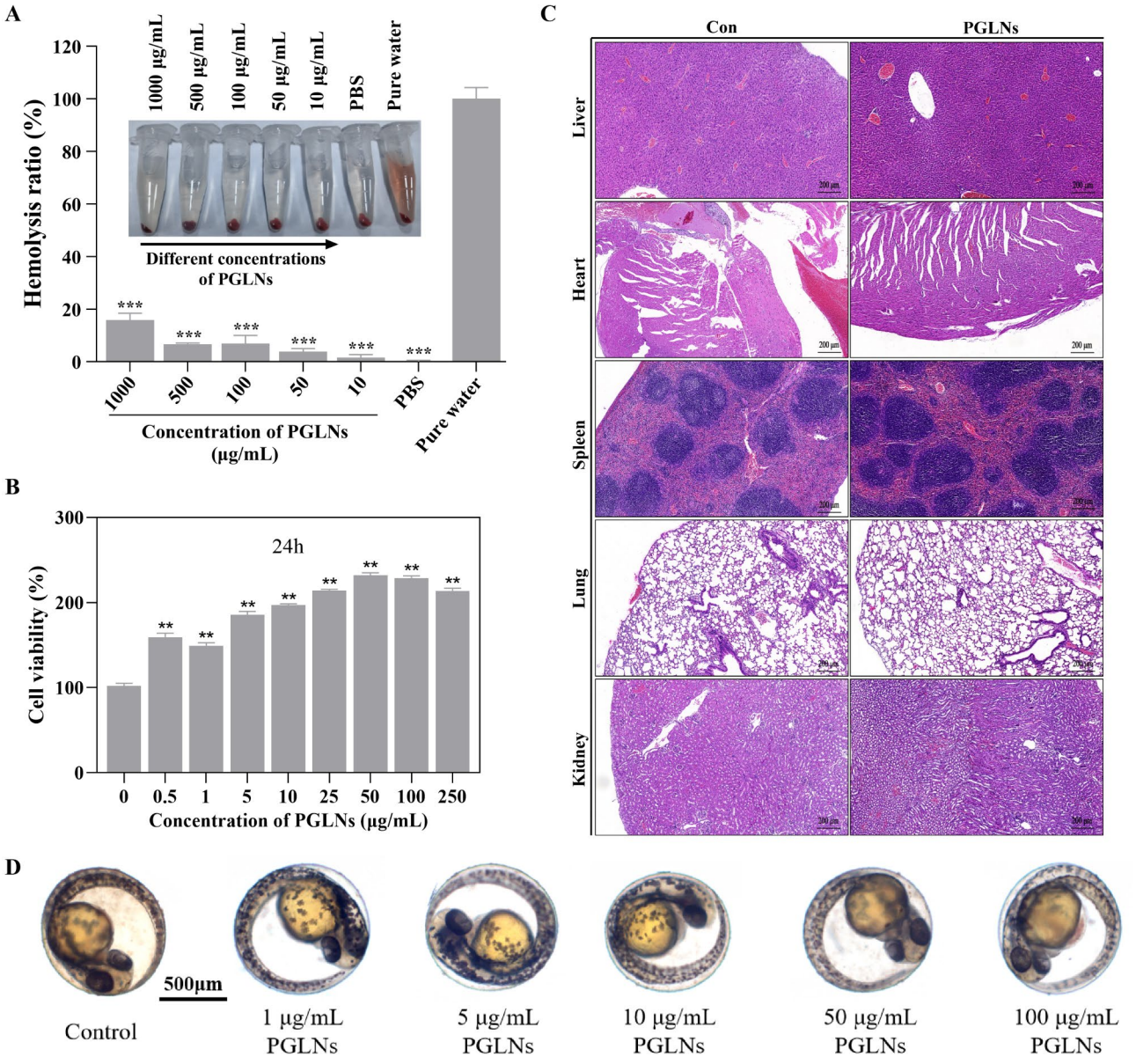

Fig. 4 Biosafety assessment of PGLNs. (A) Hemolysis activity of PGLNs at different concentrations (n = 3). (B) Cell activity after RAW264.7 cells were incubated with different concentrations of PGLNs for 24 hours (n = 6). (C) H&E staining results of liver, heart, spleen, lung and kidney tissue slices (normal control vs. PGLNs group). Scale: 200μm. (D) Zebrafish fertilized eggs after intervention with different concentrations of PGLNs for 1 day. Scale: 500 μm

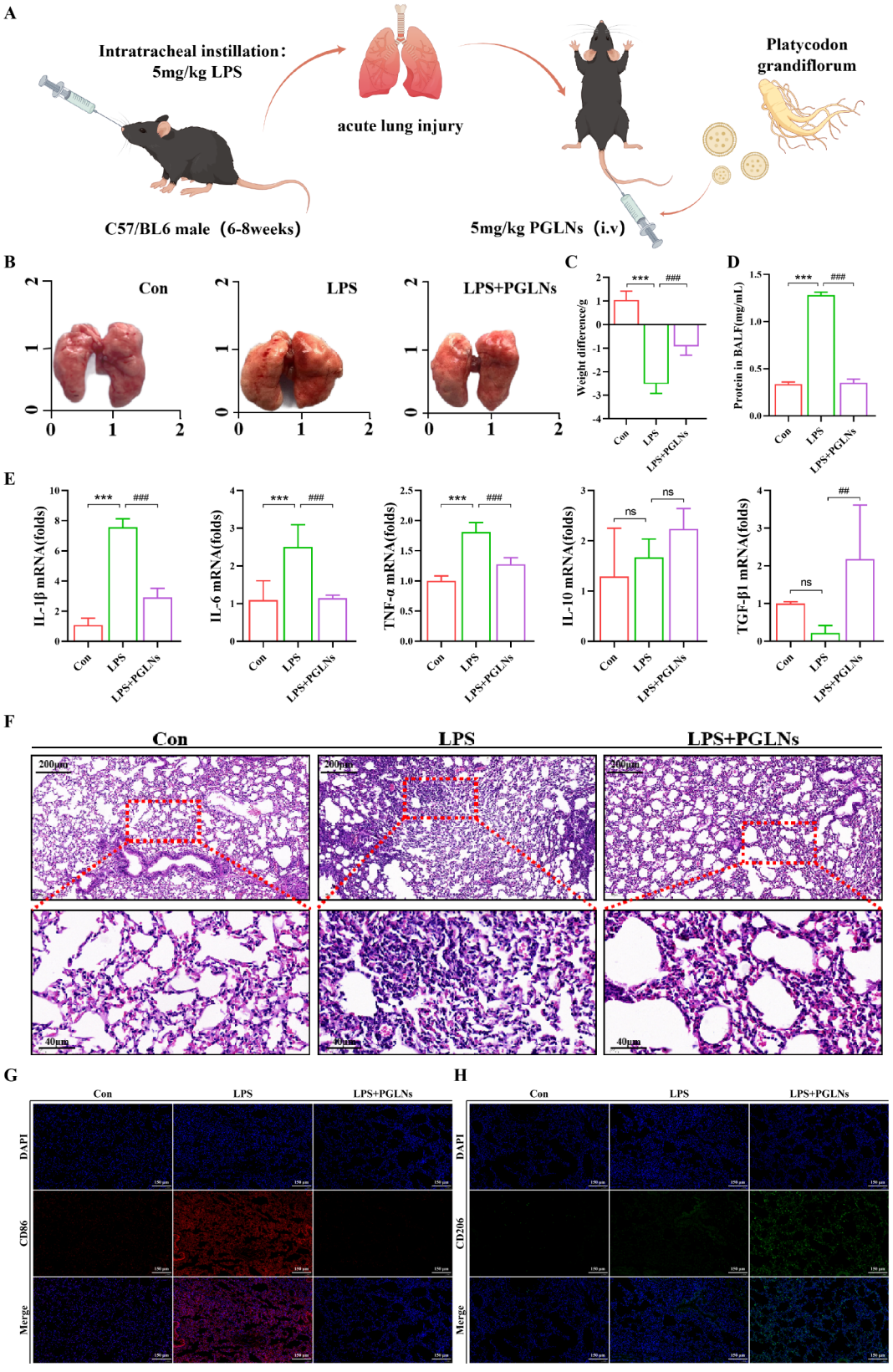

Fig. 5 (See legend on next page.)

(See figure on previous page.)

Fig. 5 PGLNs alleviated LPS-induced ALI in mice, which may be related to the regulation of macrophage polarization. (A) Schematic diagram of LPS and PGLNs administration regimens in ALI mice. (B) Differences in body weight between the LPS group and LPS+PGLNs group (n = 5). (C) Macroscopic images of mouse lung tissues in each group. Unit: cm. (D) Protein concentration in the alveolar lavage fluid of mice detected by BCA (n = 4). (E) mRNA levels of IL-1β, IL-6, TNF-α, IL-10 and TGF-β1 in mouse lung tissues detected by RT-qPCR (n = 4). (F) H&E staining results of mouse lung sections. Scale: 200μm and 40μm. (G) Fluorescence expression of M1 pro-inflammatory macrophage marker CD86 and (H) M2 anti-inflammatory macrophage marker CD206 in mouse lung tissues detected by tissue immunofluorescence. Scale: 150 μm

of 1, 5, 10, 50, and 100 μg/mL, respectively. The results showed that the morphology of zebrafish larvae exhibited no significant differences after PGLNs intervention compared to the Con group, and no abnormal phenotype was observed, suggesting that PGLNs did not produce obvious toxicity at the tested concentrations (Fig. 4D). In summary, these results indicate good biocompatibility of PGLNs and provide a safety basis for the administration of PGLNs as a natural drug preparation.

Treatment of LPS-induced ALI mice with PGLNs

To explore the anti-inflammatory effect of PGLNs, we first constructed a mouse pulmonary inflammation model via intratracheal infusion of LPS and then administered PGLNs through tail vein to observe the therapeutic effect of PGLNs (Fig. 5A). The results showed that compared to the Con group, the LPS-stimulated mice had remarkedly reduced body weight, which was significantly alleviated after PGLNs intervention (Fig. 5B). Consistently, after LPS stimulation, the lung tissues of mice manifested obvious hyperemia and edema, increased volume, and significantly elevated total protein in the alveolar lavage fluid. PGLNs intervention greatly improved the hyperemia and edema of the lung tissues, and significantly reduced the total protein content in the alveolar lavage fluid (Fig. 5C, D). Moreover, H&E staining results showed that the lung tissue structure was obviously disturbed after LPS stimulation, presenting with thickened alveolar wall and narrowed or disappeared alveolar cavity, accompanied by a large amount of exudation and inflammatory cell infiltration. PGLNs treatment significantly alleviated the pathological changes in mouse lung tissues, with the alveolar hemorrhage, interstitial edema and inflammatory cell infiltration obviously reduced or even disappeared (Fig. 5F). In addition, in LPS-stimulated mice, PGLNs significantly downregulated the mRNA expression levels of lung pro-inflammatory factors including IL-1β, IL-6, and TNF-α, and upregulated the mRNA expression level of TGF-β1 (Fig. 5E). These results indicate that PGLNs treatment can repair inflammatory injury and improve the pathological changes in mouse lung tissues, suggesting a protective effect of PGLNs on LPS-induced ALI in mice.

Macrophages are considered the first line of defense against invading pathogens and serve as coordinators of immune and inflammatory responses [20]. In this study, we found that PGLNs had a regulatory effect on alveolar macrophages in mouse lung tissues. Immunofluorescence results showed that the fluorescence intensity of M1 marker CD86 was high under LPS stimulation, while that of M2 marker CD206 was much lower in mouse lung tissues. Following PGLNs intervention, the fluorescence intensity of M1 marker CD86 was significantly reduced, while that of M2 marker CD206 showed the opposite trend (Fig. 5G, H). Therefore, we hypothesized that PGLNs might achieve their protective effect against LPS-induced ALI in mice by regulating the polarization of macrophages. Subsequently, we conducted in vitro experiments to further verify this hypothesis.

PGLNs regulate the polarization of RAW264.7 cells

We constructed an LPS-induced inflammatory injury model of RAW264.7 cells to investigate the role of PGLNs in regulating macrophage polarization. Firstly, the PGLNs were labeled with PKH67, and then co-incubated with RAW264.7 cells for 24 h. Laser confocal results showed that PKH67-labeled PGLNs and RAW264.7 cells were significantly co-located, and most PGLNs were fluorescently located in the cytoskeleton, indicating that RAW264.7 cells can effectively take up PGLNs (Fig. 6A). Subsequently, RAW264.7 cells were intervened by LPS for 24 h, and CCK8 results showed that LPS at different concentrations inhibited the activity of RAW264.7 cells to varying degrees. In the follow-up experiment, we constructed an inflammatory cell model using 1 μg/mL LPS (Fig. 6B). Consistent with the in vivo results, PGLNs significantly reduced the mRNA expression levels of pro-inflammatory factors IL-1β and IL-6 and increased the mRNA expression level of IL-10 in the LPS-stimulated cell model, indicating that PGLNs can effectively improve LPS-induced inflammatory cell injury in vitro (Fig. 6C). In addition, RT-qPCR results revealed that PGLNs significantly reduced the mRNA expression level of M1 pro-inflammatory cell marker iNOS and increased that of M2 anti-inflammatory cell marker Arg-1 in the LPS-stimulated cell model (Fig. 6D). Besides, the results of cellular immunofluorescence showed that the fluorescence intensity of M1 proinflammatory cell marker CD86 was significantly enhanced under LPS stimulation, while that of M2 anti-inflammatory cell marker CD206 was not significant. After PGLNs intervention, the changes in fluorescence intensity were reversed (Fig. 6E). The effect of PGLNs on the polarization of macrophages was analyzed

by flow cytometry, and the results showed the same trend (Fig. 6F).

Metabolic analysis of macrophage polarization regulated by PGLNs

PGLNs influence the metabolic disorder of LPS-induced RAW264.7 cells

In order to better understand the mechanism of PGLNs in regulating the LPS-induced inflammation and polarization of RAW264.7 cells, we identified the primary and secondary metabolites in the samples by employing the broad targeted metabolome technology of the UPLC-MS platform, and explored the changing patterns in cell metabolites after different treatments.

The non-targeted metabolomics analysis is illustrated in Fig. 7A. A total of 1,588 substances were identified by comparing with the metabolomics database (Fig. 7B), including 457 lipids and lipid-like molecules, 77 organic acids and derivatives, 151 organoheterocyclic compounds, 72 benzenoids, 108 organic oxygen compounds, 58 phenylpropanoids and polyketides, 20 organic nitrogen compounds, 79 nucleosides, nucleotides and analogues, and 11 alkaloids and derivatives.

The overall changing patterns in each group were observed by the PCA method, and the results showed that all samples were distributed within 95% confidence intervals, indicating that the PCA model was reliable (Fig. 7C). PCA and OPLS-DA (Fig. 7D-E) analyses among all groups indicated that the Con group was significantly separated from the LPS group, and the LPS group was significantly different from the LPS + PGLNs group. Then, OPLS-DA permutation test was performed to check the reliability of the OPLS-DA model, and it was found that the model had satisfactory fitness and prediction ability (Fig. 7F). In summary, the above results indicate that PGLNs intervention can influence the metabolic disorder of LPS-induced RAW264.7 cells, which was further confirmed by cluster analysis (Fig. 7G).

Analysis of differential metabolites in RAW264.7 cells after treatment by LPS and LPS + PGLNs

Combined with the *P*-value and magnitude of metabolite differences, the variability of metabolite changes among various groups was visualized, and the differences in Con vs. LPS and LPS vs. LPS + PGLNs were screened by integrating the VIP values obtained from the OPLS-DA model, which yielded 594 differential metabolites for Con vs. LPS and 287 differential metabolites for LPS vs. LPS + PGLNs groups.

Then, PCA analysis, OPLS-DA analysis and OPLS-DA permutation test were performed to analyze the differences between various groups. The results showed that the differences for Con vs. LPS groups and LPS vs. LPS + PGLNs groups were significantly separated (Fig. 8A-C), and the samples were clustered together. The variability of metabolite changes between groups was visualized by combining the *P*-value and the magnitude of metabolite differences (Fig. 8D). This showed that the substances in Con vs. LPS groups and in LPS vs. LPS + PGLNs groups represented the inter-group variability well. Visual analysis of the differential metabolites identified by cluster analysis revealed that the metabolites of Con vs. LPS groups and LPS vs. LPS + PGLNs groups were significantly different (Fig. 8E); the differential metabolites for Con vs. LPS groups were mainly enriched in alkaloids and derivatives, benzenoids, nucleosides, nucleotides and analogues, organic acids and derivatives, and organic nitrogen compounds (Fig. 9A), while the differential metabolites for LPS vs. LPS + PGLNs groups were mainly enriched in benzenoids, lipids and lipid-like molecules, nucleosides, nucleotides and analogues, organic acids and derivatives, organic oxygen compounds, and organoheterocyclic compounds (Fig. 9B). In addition, bubble maps of differential metabolite KEGG enrichment factor for Con vs. LPS groups and LPS vs. LPS + PGLNs groups showed that the mechanism how LPS exerts its effects was mainly associated with the purine metabolism, pyrimidine metabolism, amino sugar and nucleotide sugar metabolism, and pantothenate and CoA biosynthesis (Fig. 8F). The differences in PGLNs regulation were mainly related to linoleic acid metabolism, primary bile acid biosynthesis, glycerophospholipid metabolism, and biosynthesis of unsaturated fatty acids (Fig. 8G). In summary, these results suggest that PGLNs regulate the metabolic abnormalities in LPS-induced RAW264.7 cells via different metabolic intermediates.

Potential biomarkers of PGLNs for the treatment of LPS-induced RAW264.7 cell inflammation

To further examine the metabolite changes after PGLNs intervention, we summarized all the differential metabolites identified and determined the differences in metabolites between Con and LPS groups, as well as between LPS and LPS + PGLNs groups. In the OPLS-DA model, variables with VIP score > 1 and T-test *P* value < 0.05 were considered differential metabolites, and a total of 52 differential metabolites were obtained, including 27 upregulated ones and 25 downregulated ones (Table 2). We then evaluated the intra-group clustering and inter-group separation of these 52 differential metabolites among CON, LPS and LPS + PGLNs groups by employing the PCA model, clustering heat map and differential metabolite analysis (Fig. 10A-D).

The results of heat map analysis showed that there were significant differences in metabolite levels between the LPS and LPS + PGLNs groups, and the LPS + PGLNs group had a tendency to recover to levels of the Con group (Fig. 10B). Differential metabolite analysis showed

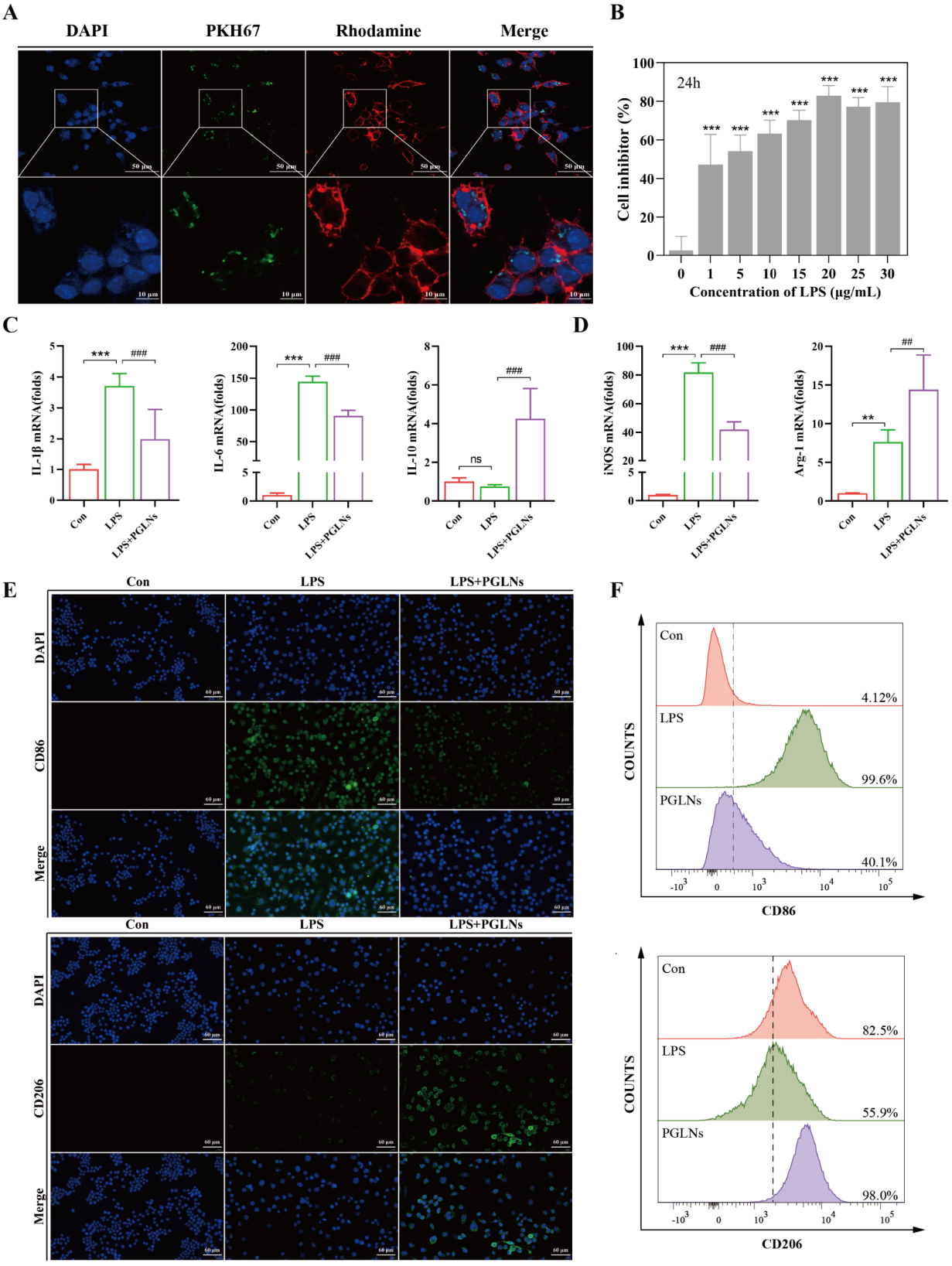

Fig. 6 PGLNs regulate macrophage polarization in vitro. (A) Laser confocal images. Uptake of PKH67-labeled PGLNs by RAW264.7 cells in vitro. Scale: 50 and 10 μm. (B) Activity of RAW264.7 cells induced by LPS at different concentrations for 24 hours (n = 4). (C) mRNA levels of IL-1β, IL-6 and IL-10 (n = 4). (D) mRNA levels of iNOS and Arg-1 (n = 4). (E) Fluorescence expression of M1 proinflammatory macrophage marker CD86 and M2 anti-inflammatory macrophage marker CD206. Scale: 60μm. Data analysis using ImageJ software. (F) Flow cytometry analysis of RAW264.7 cells

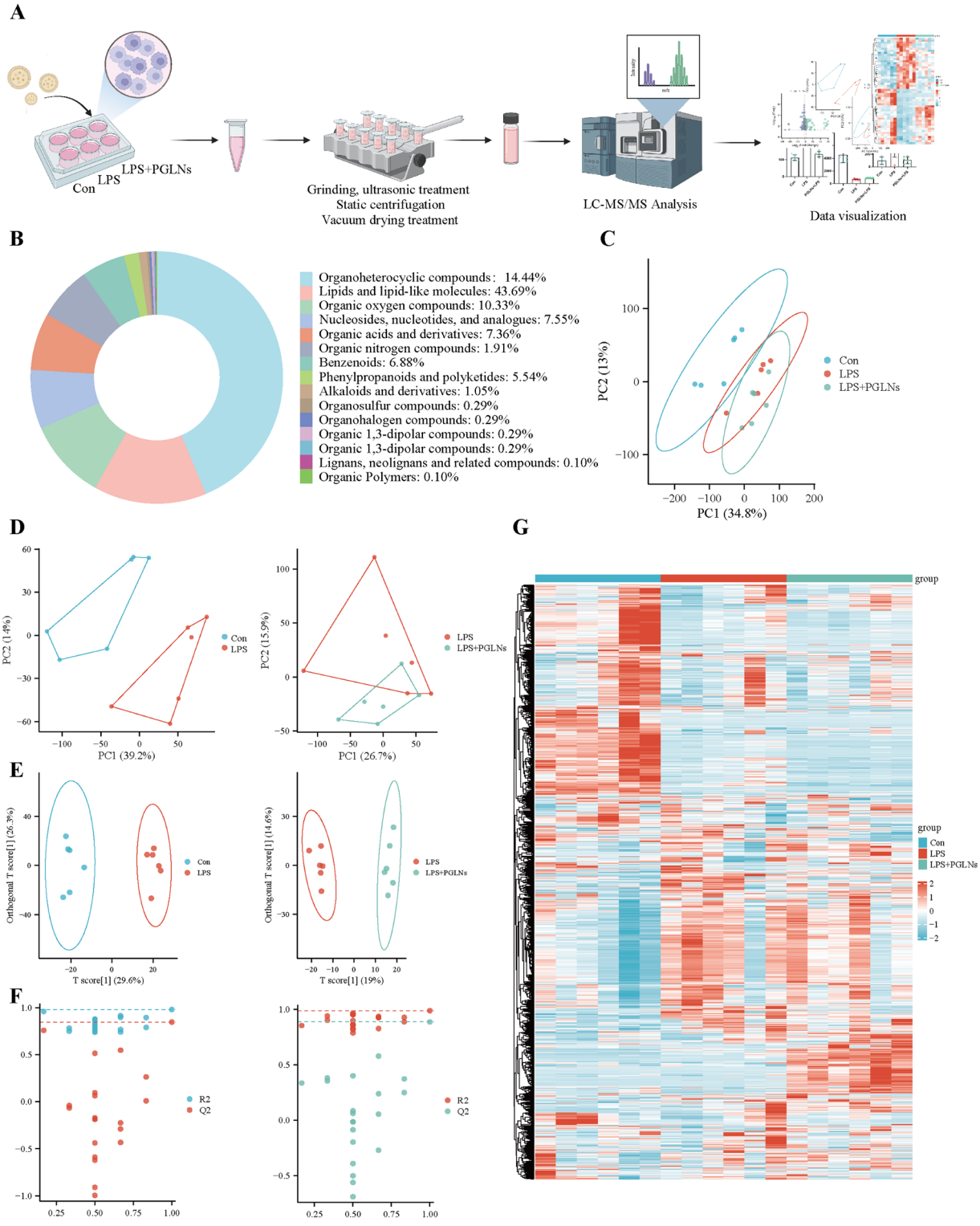

Fig. 7 PGLNs influenced the metabolic disorder of LPS-induced RAW264.7 cells. (**A**) Illustration of metabolomics analysis. (**B**) Quantity and classification of metabolites. (**C**) PCA score plots for various groups (Con, LPS and LPS + PGLNs). (**D**) PCA score plots for Con vs. LPS and LPS vs. LPS + PGLNs. (**E**) OPLS-DA score plots for Con vs. LPS and LPS vs. LPS + PGLNs. (**F**) OPLS-DA permutation test for Con vs. LPS and LPS vs. LPS + PGLNs. (**G**) Heatmap of hierarchical cluster analysis of metabolite changes ("red" and "blue" represent increased and decreased metabolite contents, respectively)

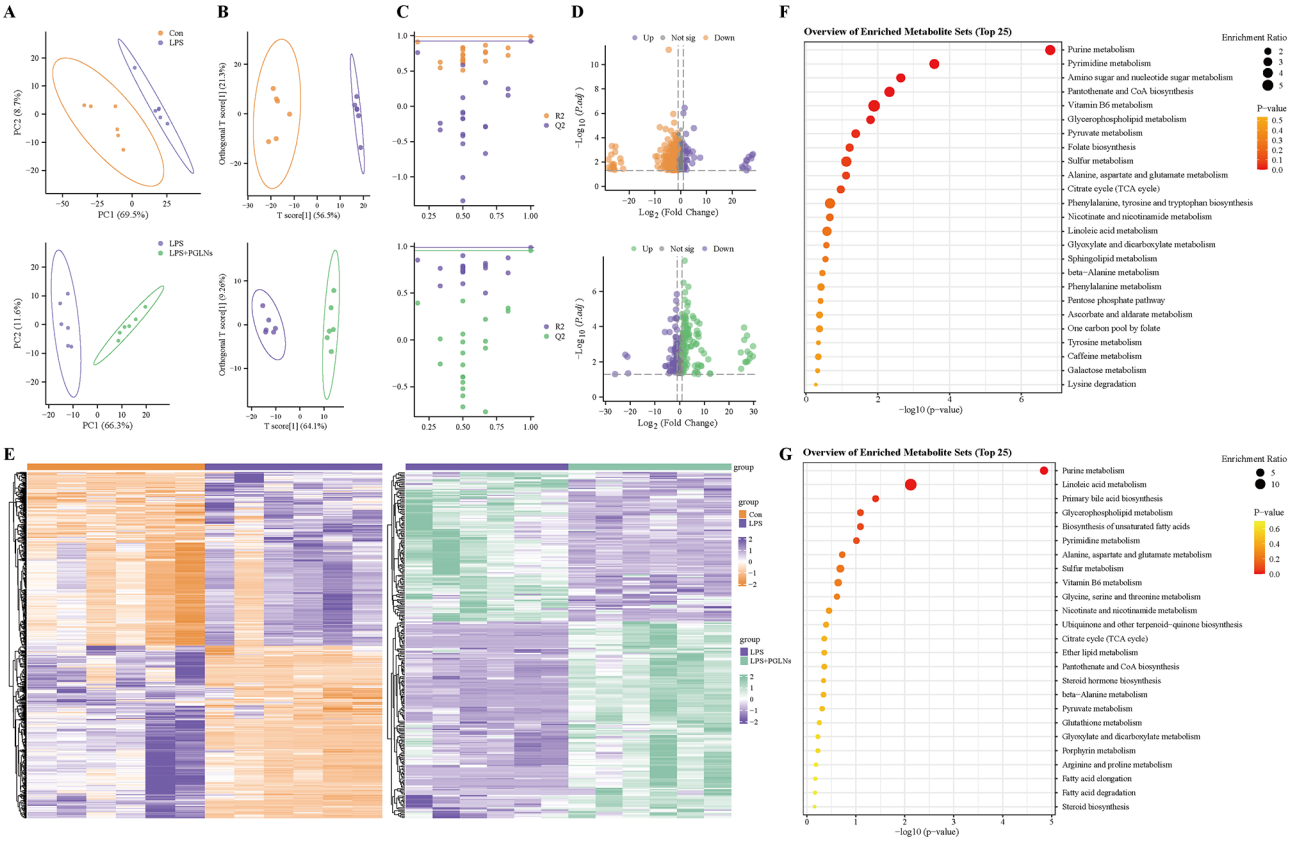

Fig. 8 Analysis of differential metabolites in RAW264.7 cells after treatment by LPS and LPS + PGLNs. (**A**) PCA score plots of different metabolites for Con vs. LPS groups, and LPS vs. LPS + PGLNs groups. (**B**) OPLS-DA score plots of different metabolites for Con vs. LPS groups and LPS vs. LPS + PGLNs groups. (**C**) OPLS-DA permutation test of different metabolites for Con vs. LPS groups and LPS vs. LPS + PGLNs groups. (**D**) Volcano plot analysis of Con vs. LPS groups and LPS vs. LPS + PGLNs groups. (**E**) Heatmap of differential metabolites for Con vs. LPS groups and LPS vs. LPS + PGLNs groups. (**F**) Bubble map of differential metabolite KEGG enrichment factor for Con vs. LPS groups. (**G**) Bubble map of differential metabolite KEGG enrichment factor for LPS vs. LPS + PGLNs groups

that the 52 metabolites exhibiting abnormalities after LPS stimulation were all reversed to varying degrees after PGLNs intervention. Specifically, 18 metabolites were almost restored to normal levels. Moreover, the difference multiple of D-Glucosamine was much higher than that of other metabolites (Fig. 10C-D). In summary, these results indicate that PGLNs can correct the abnormal metabolite levels in RAW264.7 cells induced by LPS to varying degrees.

Analysis of key metabolites of PGLNs in the treatment of LPS-induced RAW264.7 cell inflammation

We further screened out 13 key differential metabolites, whose basic characteristics and metabolic pathways are summarized in Table 3. Then, pathway analysis was conducted using MetaboAnalyst 4.0 and KEGG by referring to the related literature in order to identify the metabolic pathways closely involved in the pharmacological mechanisms of PGLNs (Fig. 11A-B). The results showed that the metabolic biomarkers of PGLNs were mainly involved in the glycerophospholipid metabolism, vitamin B6 metabolism, ether lipid metabolism, pantothenate and CoA biosynthesis, alanine, aspartate and glutamate metabolism, glycine, serine and threonine metabolism, as well as amino sugar and nucleotide sugar metabolism. The changes in 13 potential metabolites in the cells after PGLNs intervention were quantitatively analyzed, as shown in Fig. 11C.

After performing functional analysis of the metabolic pathways involved in the pharmacological mechanisms of PGLNs, the metabolic pathway relationship diagram was drawn (Fig. 12). The results showed that PGLNs might alleviate pulmonary inflammation by regulating the polarization of macrophages via the amino acid and lipid metabolism and the glycolysis pathway.

Discussion

ALI is a life-threatening respiratory disease with a high mortality rate and poor prognosis. Supportive treatment is one of the common clinical strategies for ALI, but it often produces adverse reactions such as elevated blood sugar, weight gain, hypertension, bone calcium loss, and

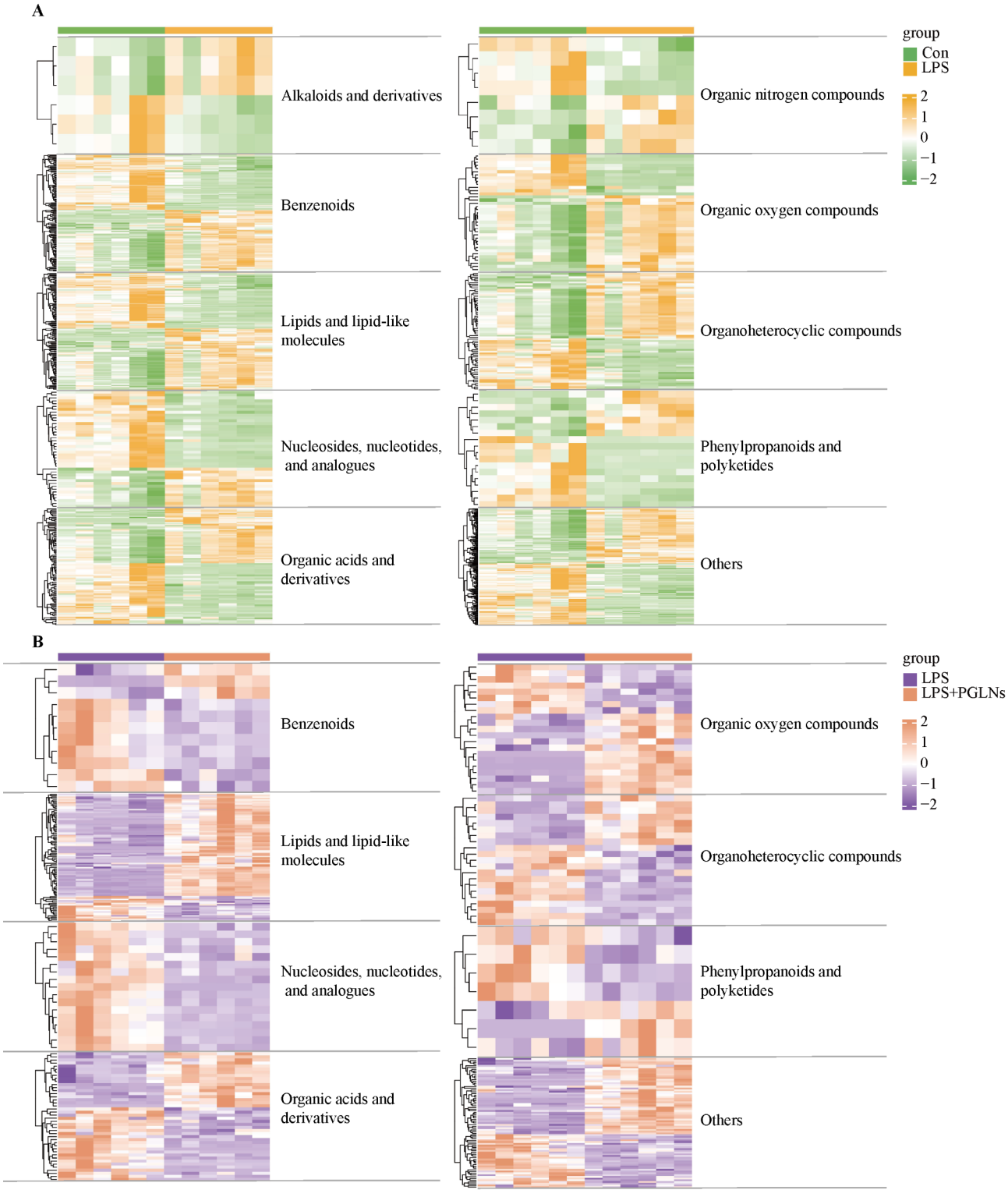

Fig. 9 Clustering heatmap of differential metabolites for Con vs. LPS (**A**) and LPS vs. LPS + PGLNs (**B**)

developmental delay in children [2, 21]. Therefore, development of new reagents with low toxicity, high safety and good therapeutic effects is of great significance for patients with ALI.

PG, available in both fresh and dried forms, is a traditional Chinese herbal medicine widely used in treating lung-related diseases [22]. The fresh use of herbal medicine is one of the characteristics of traditional Chinese

Table 2 Differential metabolites in the treatment of RAW264.7 cell inflammation by PGLNs

Metabolite	Formula	Retention time (min)	m/z	Error (ppm)	Pvalue		VIP		Super_class	Trend	
					C_vs_L	L_vs_P	C_vs_L	L_vs_P		C_vs_L	L_vs_P
Isavuconazole	$C_{22}H_{17}F_2N_5OS$	0.80	436.10	-4.23	0.00	0.01	1.51	1.90	Benzenoids	up	down
Glucoberteroin	$C_{13}H_{25}NO_9S_3$	0.81	480.07	-0.57	0.01	0.02	1.46	1.71	Organic oxygen compounds	up	down
Pantothenate	$C_9H_{17}NO_5$	1.91	218.11	8.06	0.00	0.04	1.64	1.28	Organic oxygen compounds	down	up
2- [(2R,5Z)-2-Carboxy-4-methylthiazo-3- 5(2 H)-ylidene]ethyl phosphate	$C_7H_{10}NO_6PS$	11.22	287.97	1.91	0.02	0.04	1.36	1.33	--	up	down
3,4-Dihydroxyphthalate	$C_8H_6O_6$	11.23	232.99	10.88	0.02	0.01	1.27	1.60	--	up	down
Phosphonoacetate	$C_2H_5O_5P$	11.26	174.96	9.15	0.00	0.02	1.72	1.47	Organic acids and derivatives	up	down
CDP-ethanolamine	$C_{11}H_{20}N_4O_{11}P_2$	2.30	467.04	19.20	0.00	0.01	1.58	1.49	Nucleosides, nucleotides, and analogues	up	down
GDP-beta-L-colitose	$C_{16}H_{25}N_5O_{14}P_2$	2.30	618.08	-10.41	0.00	0.04	1.61	1.28	--	up	down
S-(2-Furanylmethyl) methanethioate	$C_6H_6O_2S$	2.36	283.01	-1.03	0.00	0.03	1.59	1.35	Organoheterocyclic compounds	up	down
Tolmetin glucuronide	$C_{21}H_{23}NO_9$	4.39	454.11	-3.96	0.02	0.01	1.32	1.73	Organic acids and derivatives	up	down
4- (Cyclohexylamino)-2-hydroxy-1-5- propanesulfonic acid	$C_9H_{19}NO_4S$	4.62	236.10	5.08	0.01	0.02	1.29	1.39	Organic nitrogen compounds	up	down
Aurachin B	$C_{25}H_{33}NO_2$	7.26	424.25	-8.95	0.00	0.02	1.47	1.53	--	down	up
Sambutoxin	$C_{28}H_{39}NO_4$	7.46	474.26	-0.31	0.05	0.02	1.13	1.55	Lipids and lipid-like molecules	down	up
Retaspimycin	$C_{31}H_{45}N_3O_8$	7.47	586.31	-0.53	0.03	0.04	1.26	1.44	Phenylpropanoids and polyketides	down	up
Glu-Ile-Leu-Asp-Val	$C_{26}H_{45}N_5O_{10}$	7.85	632.31	-0.20	0.01	0.00	1.43	2.03	Organic acids and derivatives	down	up
LysoPC(22:5(7Z,10Z,13Z,16Z,19Z)/0:0)	$C_{30}H_{52}NO_7P$	8.03	614.34	-7.07	0.01	0.00	1.38	2.02	Lipids and lipid-like molecules	down	up
LysoPI(18:1(9Z)/0:0)	$C_{27}H_{51}O_{12}P$	8.21	619.29	0.92	0.01	0.01	1.42	1.61	Lipids and lipid-like molecules	down	up
Avermectin A1a	$C_{49}H_{74}O_{14}$	8.48	921.48	6.48	0.00	0.00	1.55	1.79	Phenylpropanoids and polyketides	up	down
PGP(a-17:0/20:3(8Z,11Z,14Z)-2OH(5,6))	$C_{43}H_{80}O_{15}P_2$	8.59	919.47	-0.62	0.02	0.01	1.22	1.60	--	up	down
(R)-Pronuciferine	$C_{19}H_{21}NO_3$	8.84	621.30	9.14	0.04	0.00	1.18	1.77	Alkaloids and derivatives	down	up
PE(P-16:0/PGF1alpha)	$C_{41}H_{78}NO_{10}P$	9.17	774.52	-5.28	0.00	0.02	1.58	1.54	--	up	down
2-Oxo-3-hydroxy-4-phosphobutanoate	$C_4H_7O_8P$	0.56	248.96	28.27	0.00	0.04	1.47	1.31	Organic acids and derivatives	up	down
PE(16:0/18:2(9Z,12Z))	$C_{39}H_{74}NO_8P$	9.51	714.50	-6.61	0.00	0.04	1.64	1.45	Lipids and lipid-like molecules	up	down
xi-p-Mentha-1(7),2-dien-4-ol	$C_{10}H_{16}O$	9.58	303.23	1.38	0.00	0.00	1.56	2.14	Lipids and lipid-like molecules	down	up
D-Glucosamine	$C_6H_{13}NO_5$	9.58	403.16	3.91	0.02	0.00	1.40	2.02	Organic oxygen compounds	down	up
1-Fluoro-3-(2-methylphenyl)uracil	$C_{11}H_9FN_2O_2$	9.74	439.12	4.16	0.02	0.04	1.29	1.35	Organoheterocyclic compounds	up	down
N(gamma)-Acetyldiaminobutyrate	$C_6H_{12}N_2O_3$	0.64	195.05	-11.35	0.02	0.02	1.29	1.49	--	down	up
Atrazine	$C_8H_{14}ClN_5$	4.18	254.06	3.54	0.01	0.00	1.46	1.99	Organoheterocyclic compounds	down	up
N-Acetylaspartylglutamylglutamate	$C_{16}H_{23}N_3O_{11}$	4.39	456.13	8.26	0.03	0.03	1.32	1.52	--	up	down
1-Methylinosine	$C_{11}H_{14}N_4O_5$	5.55	324.13	-1.16	0.00	0.00	1.56	1.85	Nucleosides, nucleotides, and analogues	up	down
Choline	$C_5H_{13}NO$	0.61	104.11	7.06	0.00	0.00	1.52	2.06	Organic nitrogen compounds	down	up
Glycerophosphocholine	$C_8H_{20}NO_6P$	0.61	258.11	1.15	0.00	0.00	1.79	2.20	Lipids and lipid-like molecules	up	down
N-Methylhydantoin	$C_4H_6N_2O_2$	0.64	132.08	2.01	0.00	0.00	1.79	2.18	Organoheterocyclic compounds	up	down
3- Methyl-8-(2-methylpropyl)-7 H-4- purine-2,6-dione	$C_{10}H_{14}N_4O_2$	0.70	222.11	7.72	0.00	0.05	1.58	1.26	Organoheterocyclic compounds	up	down

Table 2 (continued)

Metabolite	Formula	Retention time (min)	m/z	Error (ppm)	Pvalue		VIP		Super_class	Trend	
					C_vs_L	L_vs_P	C_vs_L	L_vs_P		C_vs_L	L_vs_P
O-Acetylcarnitine	$C_9H_{18}NO_4^+$	0.75	204.12	0.56	0.00	0.00	1.75	1.92	Lipids and lipid-like molecules	down	up
Gly Tyr	$C_{11}H_{14}N_2O_4$	0.80	239.09	-0.56	0.00	0.03	1.58	1.54	--	up	down
hydroxydeoxyguanosine	$C_{10}H_{13}N_5O_5$	0.81	306.08	1.81	0.03	0.01	1.20	1.76	Organoheterocyclic compounds	down	up
Pantothenic Acid	$C_9H_{17}NO_5$	1.90	220.12	0.27	0.00	0.00	1.71	1.80	Organic oxygen compounds	down	up
p-Coumaroylagmatine	$C_{14}H_{20}N_4O_2$	8.04	570.35	-2.58	0.00	0.00	1.50	2.01	--	down	up
PE(16:0/0:0)	$C_{21}H_{44}NO_7P$	8.06	454.29	-1.68	0.00	0.03	1.53	1.53	Lipids and lipid-like molecules	down	up
Deoxycholylproline	$C_{29}H_{47}NO_5$	8.18	528.31	3.95	0.00	0.04	1.52	1.39	--	down	up
LysoPC(18:0/0:0)	$C_{26}H_{54}NO_7P$	8.32	546.36	4.68	0.00	0.05	1.64	1.41	Lipids and lipid-like molecules	down	up
Deoxycholylcitrulline	$C_{30}H_{51}N_3O_6$	8.44	572.37	7.36	0.02	0.00	1.31	1.99	--	down	up
3-dehydrosphinganine (C20)	$C_{20}H_{42}NO_2$+	8.50	367.28	-2.21	0.01	0.00	1.33	1.93	Organic oxygen compounds	up	down
N1-Acetylspermidine	$C_9H_{21}N_3O$	8.64	413.30	5.08	0.00	0.05	1.57	1.32	Organic acids and derivatives	up	down
9(Z),11(E)-Conjugated Linoleic Acid	$C_{18}H_{32}O_2$	9.23	303.23	-1.88	0.00	0.00	1.58	2.21	--	down	up
dehydroabietadienol	$C_{20}H_{30}O$	9.27	287.24	0.13	0.00	0.00	1.60	2.13	--	down	up
(E, E)-3,7,11-Trimethyl-2,6,10-dodecatrienyl propionate	$C_{18}H_{30}O_2$	9.28	279.23	1.45	0.01	0.01	1.38	1.83	--	down	up
16,16-dimethyl-PGA1	$C_{22}H_{36}O_4$	9.48	329.25	5.71	0.02	0.00	1.35	2.01	--	down	up
2- Hydroxy-4-oxo-5,12-3- heneicosadien-1-yl acetate	$C_{23}H_{40}O_4$	9.55	381.30	7.52	0.03	0.00	1.29	2.25	Lipids and lipid-like molecules	down	up
Osmundalin	$C_{12}H_{18}O_8$	9.57	273.10	6.76	0.00	0.02	1.45	1.53	Organic oxygen compounds	up	down
PC(16:0/0:0)[U] / PC(16:0/0:0)[rac]	$C_{24}H_{50}NO_7P$	9.72	496.34	3.76	0.00	0.03	1.62	1.46	--	down	up

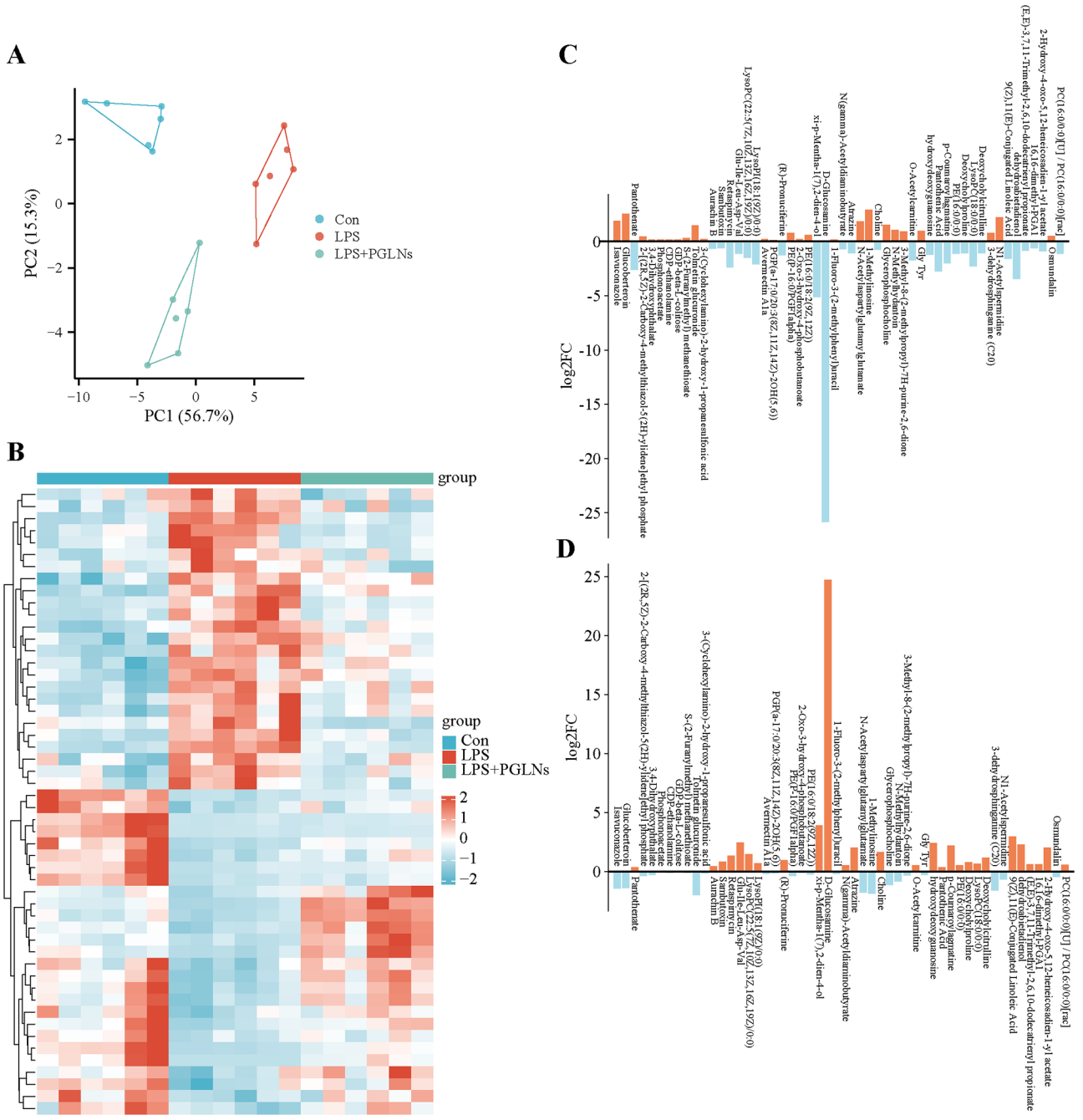

Fig. 10 Potential biomarkers of PGLNs for the treatment of LPS-induced RAW264.7 cell inflammation. (**A**) PCA score plots of potential biomarkers for differential metabolites among various groups (Con, LPS, and LPS + PGLNs). (**B**) Heatmap of hierarchical cluster analysis of potential biomarkers for Con vs. LPS, and LPS vs. LPS + PGLNs ("red" and "blue" represent increased and decreased metabolite contents, respectively). (**C**) Multiples of difference in potential biomarkers for Con vs. LPS. (**D**) Multiples of difference in potential biomarkers for LPS vs. LPS + PGLNs

medicine in the treatment of inflammation and fever diseases. As early as in the ancient Chinese medicine book "Shennong Herbal Classic", it has pointed out that fresh herbal medicine has good therapeutic effects, which can be better than those of dried medicinal plants. Unlike the widely recognized method of boiling and decocting, fresh herbal medicine contains rich plant juices that help retain the active substances to the maximum extent. However, the application of fresh herbal medicine has been severely limited due to restrictions in seasonality and preservation technology. At present, the research of fresh herbal medicine is not only a missing discipline in the field of modern medicine, but also a blind spot in the research of traditional Chinese medicine. In recent years, with the

Table 3 Summary of key differential metabolites of PGLNs in the treatment of RAW264.7 cell inflammation

Metabolite	Formula	Retention time (min)	m/z	Error (ppm)	Pvalue		VIP		Metabolic pathway	Trend	
					C_vs_L	L_vs_P	C_vs_L	L_vs_P		C_vs_L	L_vs_P
Glucoberteroin	$C_{13}H_{25}NO_9S_3$	0.81	480.07	-0.57	0.01	0.02	1.46	1.71	2-Oxocarboxylic acid metabolism	Up***	Down**
2-[(2R,5Z)-2-Carboxy-4-methylthiazol-5(2 H)-ylidene]ethyl phosphate	$C_7H_{10}NO_6PS$	11.22	287.97	1.91	0.02	0.04	1.36	1.33	Thiamine metabolism	Up**	Down*
Phosphonoacetate	$C_2H_5O_5P$	11.26	174.96	9.15	0.00	0.02	1.72	1.47	Phosphonate and phosphinate metabolism	Up****	Down*
CDP-ethanolamine	$C_{11}H_{20}N_4O_{11}P_2$	2.30	467.04	19.20	0.00	0.01	1.58	1.49	Glycerophospholipid metabolism	Up***	Down*
GDP-beta-L-colitose	$C_16H_{25}N_5O_{14}P_2$	2.30	618.08	-10.41	0.00	0.04	1.61	1.28	Biosynthesis of nucleotide sugars	Up****	Down^{ns}
Pantothenic Acid	$C_9H_{17}NO_5$	1.90	220.12	0.27	0.00	0.00	1.71	1.80	Pantothenate and CoA biosynthesis	Down****	up^{ns}
N(gamma)-Acetyldiaminobutyrate	$C_6H_{12}N_2O_3$	0.64	195.05	-11.35	0.02	0.02	1.29	1.49	Glycine, serine and threonine metabolism	Down*	Up*
2-Oxo-3-hydroxy-4-phosphobutanoate	$C_4H_7O_8P$	0.56	248.96	28.27	0.00	0.04	1.47	1.31	Vitamin B6 metabolism	Up**	down^{ns}
D-Glucosamine	$C_6H_{13}NO_5$	9.58	403.16	3.91	0.02	0.00	1.40	2.02	Amino sugar and nucleotide sugar metabolism	Down**	up^{ns}
N-Acetylaspartylglutamylglutamate	$C_{16}H_{23}N_3O_{11}$	4.39	456.13	8.26	0.03	0.03	1.32	1.52	Alanine, aspartate and glutamate metabolism	Up**	Down**
Choline	$C_5H_{13}NO$	0.61	104.11	7.06	0.00	0.00	1.52	2.06	Glycine, serine and threonine metabolism	Down**	Up**
Glycerophosphocholine	$C_8H_{20}NO_6P$	0.61	258.11	1.15	0.00	0.00	1.79	2.20	Glycerophospholipid metabolism	Up****	Down****
N-Methylhydantoin	$C_4H_6N_2O_2$	0.64	132.08	2.01	0.00	0.00	1.79	2.18	Arginine and proline metabolism	Up****	Down****

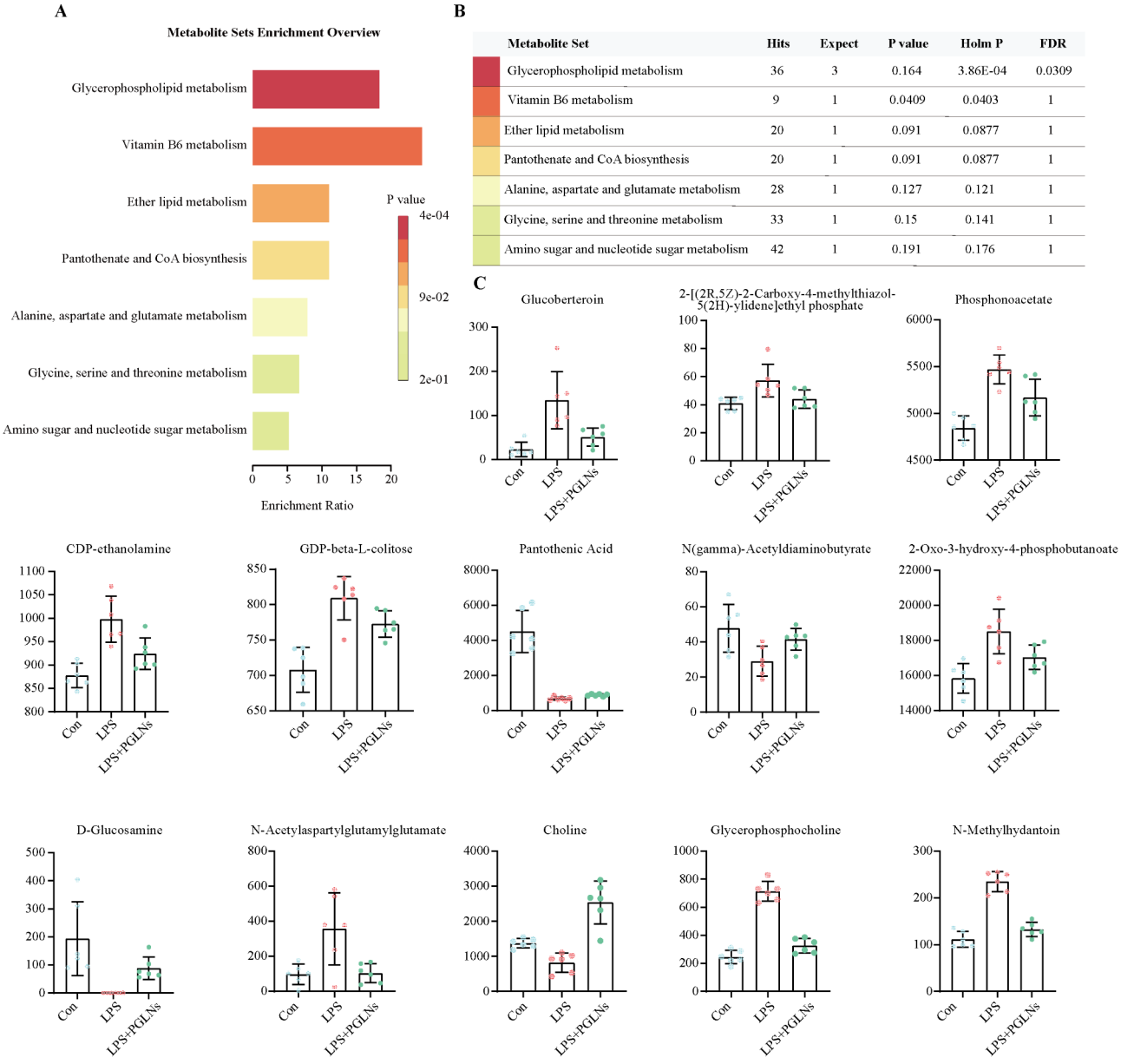

Metabolite Set	Hits	Expect	P value	Holm P	FDR
Glycerophospholipid metabolism	36	3	0.164	3.86E-04	0.0309
Vitamin B6 metabolism	9	1	0.0409	0.0403	1
Ether lipid metabolism	20	1	0.091	0.0877	1
Pantothenate and CoA biosynthesis	20	1	0.091	0.0877	1
Alanine, aspartate and glutamate metabolism	28	1	0.127	0.121	1
Glycine, serine and threonine metabolism	33	1	0.15	0.141	1
Amino sugar and nucleotide sugar metabolism	42	1	0.191	0.176	1

Fig. 11 Analysis of key metabolites of PGLNs in the treatment of LPS-induced RAW264.7 cell inflammation. (**A**) KEGG enrichment map of potential biomarkers. (**B**) Metabolic pathway enrichment information of potential biomarkers. (**C**) Quantitative analysis of key metabolites

emergence of new preservation technology, ultra-high speed centrifugation technology and nanoscale particle detection methods, the application of traditional Chinese medicine is undergoing revolutionary changes. The irreplaceability and superiority of fresh herbal medicine are drawing increasing attention and have been proven by previous research. This is of great significance for promoting the development and clinical application of fresh herbal drugs. Nonetheless, the differences between the fresh and dried forms of the same herbal medical are to be further clarified and explained.

In this study, we first used LPS to induce a mouse model of ALI and investigated the differences between fresh and dried PG in treating ALI mice. The results showed that fresh PG could significantly alleviate the weight loss of ALI mice and improve the structural disorder of lung tissues and inflammatory infiltration, indicating that fresh PG has good therapeutic effects on ALI in mice. Due to restrictions in seasonality and preservation technology, PG is mostly used in the form of dried medicine in clinical applications. However, studies have shown that the chemical composition of dried Chinese traditional medicine degrades seriously during processing, resulting in the loss of active ingredients [23]. Consistently, our results also supported that the efficacy of fresh PG was indeed better than that of dried PG, highlighting strong

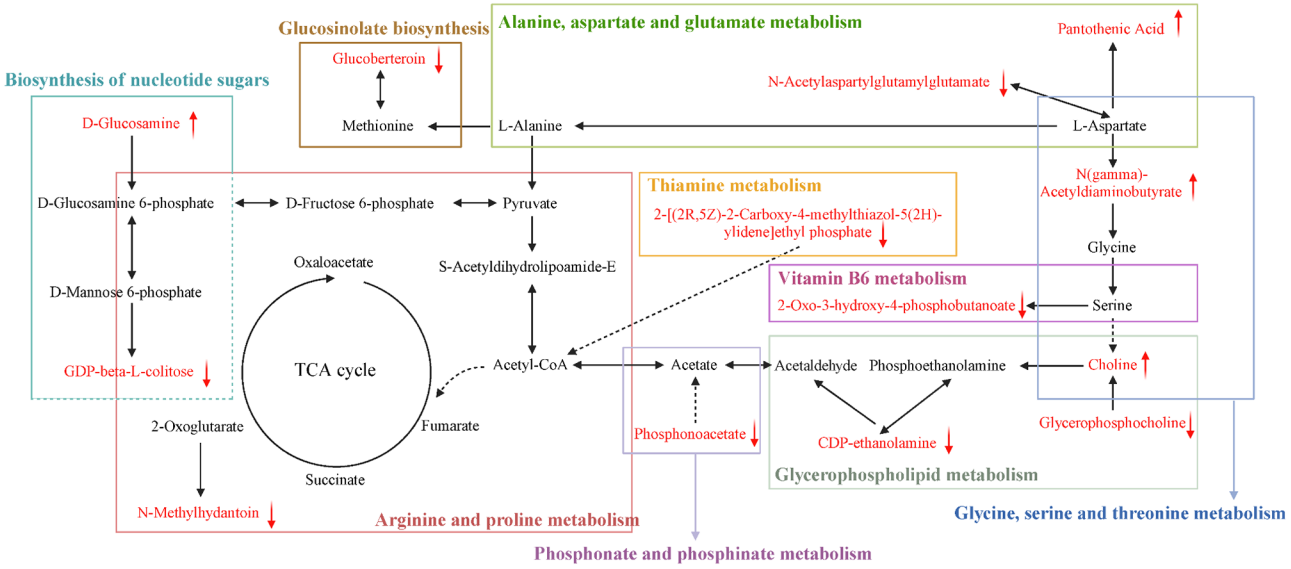

Fig. 12 Relationship diagram of metabolic pathways for the pharmacological mechanisms of PGLNs

research and application prospects of unprocessed fresh drug forms. Therefore, we further explored the active substances in fresh PG that play a protective role in lung diseases.

Plant-derived exosome-like nanoparticles are nanoscale membrane vesicles with a diameter of 40–100 nm that are actively released by fresh plant cells, playing a role in the transmission of information and substances in intercellular and interspecific communication [24–26]. Exosome-like nanoparticles derived from medicinal plants have been shown to play important roles in many aspects such as treatment of tumor, intestinal disease, and hypertension, immunity, inflammatory responses, and drug delivery. Xinyue Zhang et al. found that exosome-like nanoparticles derived from dandelion could effectively prevent hypertension caused by chronic intermittent hypoxia by regulating metabolites of gut microbes [16]. Min-zheng Zhu et al. reported that exosome-like nanoparticles from purslane promoted the proliferation of $CD4^+$ $CD8^+$ double-positive T cells, and effectively inhibited the colitis induced by dextran sodium sulfate in mice [27]. Besides, Jin-Hyeon Hwang et al. found that yam-derived exosome-like nanoparticles promoted osteoblast proliferation, thereby preventing osteoporosis in mice [28]. Based on the bioactivity and information communication of these nanoscale vesicles, we speculate that exosome-like nanoparticles derived from fresh medicinal plants may be the material basis for their better effects in drug efficacy.

In this study, we extracted and purified PGLNs using differential centrifugation and the sucrose density gradient method, and further identified and characterized their physicochemical properties and composition by electron microscopy, particle size, Zeta potential, agar-gel electrophoresis, SDS-PAGE electrophoresis and proteomic analysis. It was found that PGLNs had a nanoscale size and a vesicle-like structure, and were rich in a variety of proteins with different molecular weights and biological functions. Subsequently, to evaluate the biosafety and biocompatibility of PGLNs, we conducted multifaceted toxicological experiments in cells and animals, and the results showed that PGLNs at all tested concentrations exhibited low hemolytic activity and no toxic effects on animals, and could even promote cell proliferation. The high yield, stable extraction, and good biocompatibility of PGLNs indicate that PGLNs have a great potential as a natural nanomedicine and nanocarrier.

Further experimental results revealed that PGLNs could effectively alleviate the ALI injury of RAW264.7 cells in mice, providing a stronger evidence for PGLNs as a natural nanomedicine. Moreover, we found that PGLNs had a regulatory effect on the polarization of macrophages, which are key cells in the human innate immunity. When stimulated by different internal environments, macrophages can develop and polarize into two different phenotypes, namely pro-inflammatory M1 macrophages and anti-inflammatory M2 macrophages. The balance between the two is crucial for maintaining homeostasis [29–31]. A mass of studies have shown that macrophage polarization plays a pivotal role in the treatment of various inflammatory diseases [32–34]. Our results showed that PGLNs reduced the mRNA expression level of iNOS and the fluorescence intensity of CD86 in macrophages, but increased the mRNA expression level of Arg-1 and the fluorescence intensity of CD206 in vitro. Meanwhile, PGLNs also reduced the fluorescence intensity of CD86 and increased the fluorescence intensity of CD206 in mouse lung tissues in vivo. The results of flow cytometry

showed the same trend. These results further confirmed that PGLNs could ameliorate LPS-induced inflammatory damage by regulating the polarization of macrophages. It is worth noting that exosome-like nanoparticles derived from medicinal plants carry proteins, lipids, mRNA and pharmacodynamic substances of homologous plants, and exert drug efficacy through multiple pathways. This multi-component, multi-target pharmacological mechanism is in line with Chinese herbal medicine. Therefore, we cannot completely rule out the possibility that PGLNs may have direct effects on innate immune cells or other tissue cells other than macrophages, which deserves further investigation in future research.

Nonetheless, the specific mechanisms by which PGLNs regulate macrophage polarization to relieve pulmonary inflammation remain unclear. Therefore, we conducted non-targeted metabolomics investigations to further explore their possible mechanisms of action.

In recent years, metabolomics has made great achievements in understanding the metabolic changes during macrophage inflammation and polarization [35–37]. In this study, we employed non-targeted metabolomics for the first time to analyze the metabolomic characteristics of LPS-induced RAW264.7 cells after PGLNs intervention, which may help clarify the mechanisms of action of PGLNs in regulating the polarization of macrophages in inflammatory injury. Lipids and their metabolites are participants in complex signaling pathways, playing an important role in controlling macrophage functions. Studies have shown that lipid metabolism of macrophages can regulate the phagocytosis of macrophages and the production of inflammatory factors. Intracellular lipid droplets, in addition to storing excess intracellular lipids, can also regulate the phagocytosis in macrophages and the production of lipid-mediated factors such as leucotrienes and prostaglandins [38]. Besides, multiple metabolic intermediates in the cholesterol synthesis pathway are able to regulate the production of inflammatory factors and the antiviral function of macrophages, and the polarization of macrophages is also affected by lipids [39]. Dysfunction of glycerophospholipid metabolism reflects the metabolic changes caused by inflammatory response and oxidative stress [40, 41]. Our study revealed that three metabolites in the glycerophospholipid metabolism regulated by PGLNs were significantly recovered to normal levels, indicating that PGLNs have a prominent regulatory effect on the glycerophospholipid metabolism in LPS-induced inflammation. Choline, the parent compound of the cholines class, is an important component of lecithin and sphingomyelin, and an essential nutrient required for the synthesis of main eukaryotic phospholipids [42]. Studies have shown that choline can regulate the production of IL-1β and IL-18 in macrophages, thereby affecting the inflammation of macrophages, and that low circulating Choline levels are associated with increased inflammation [43, 44]. This is consistent with our findings, but how PGLNs affects choline levels remains to be further clarified. In summary, our metabolomics results indicate that there are significant differences in multiple lipid metabolites in macrophages after PGLNs treatment compared to those in the LPS group, and there are also differences in multiple lipid metabolic pathways in enrichment analysis. Therefore, we speculate that PGLNs may regulate macrophage polarization to alleviate pulmonary inflammation by regulating lipid metabolism pathways.

Furthermore, a large number of studies have shown that the glycolytic pathway also exerts a regulatory effect on the polarization of macrophages, which plays a critical role in the treatment of many inflammatory diseases [45, 46]. The entire process of glycolysis can be divided into two stages: the chemical initiation stage with D-glucose as the starting compound, and the energy production stage. Moreover, the biosynthesis of pantothenic acid and coenzyme A has also been identified as a major metabolic pathway. Disruption of these pathways can lead to disruption of energy supply [47, 48]. D-glucosamine, an amino sugar, is an important precursor in the biochemical synthesis of glycosylated proteins and lipids, and may promote human cartilage health. Meanwhile, D-glucosamine also acts as an inhibitor of glycolysis, and has been shown to improve the survival in sepsis mice and alleviate the lung damage and inflammation induced by sepsis [49]. In this study, 52 differential metabolites were identified in cell metabolites; among them, D-glucosamine and pantothenic acid were significantly down-regulated in LPS-stimulated cells, and were significantly recovered after PGLNs intervention. Therefore, we speculate that PGLNs may regulate macrophage polarization by regulating the glycolytic pathway, thereby ameliorating cellular inflammatory damage. Overall, our study demonstrated that PGLNs ameliorated inflammatory damage by regulating macrophage polarization in both in vitro and in vivo models of LPS-induced inflammation, and could recover LPS-induced irregular metabolism back to a more physiological state by improving inflammatory responses and lipid, nucleic acid, and glucose metabolism. These findings provide a systematic vision for the treatment of PGLNs.

Conclusions

Fresh PG can improve inflammation in the body, and exhibits a better therapeutic effect than its dried form. Consistently, the PGLNs extracted from fresh PG can improve inflammation both in vivo and in vitro. In this study, we revealed for the first time that PGLNs inhibited LPS-induced RAW264.7 macrophage inflammation and alleviated LPS-induced ALI in mice. In addition, we also

found that PGLNs promoted the expression of M2 anti-inflammatory macrophages and inhibited the expression of M1 pro-inflammatory macrophages, and could regulate macrophage metabolism in vitro, including the glycolysis, lipid and amino acid metabolic pathways.

Abbreviations

ALI	Acute Lung Injury
PG	Platycodon Grandiflorum
LPS	Lipopolysaccharide
PGLNs	Platycodon Grandiflorum exosome-Like Nanoparticles
TEM	Transmission Electron Microscopy
NTA	Nanoparticle Tracking Analysis
PBS	Phosphate-Buffered Saline
CCK-8	Cell Counting Kit-8
PF	Platycodon Fresh Products Extract
PFW	Platycodon Fresh distilled Water
PD	Dried platycodon grandiflorum extract
PDW	Platycodon Dried Distilled Water
TNF-α	Tumor Necrosis Factor-α
IL-1β	Interleukin-1β
IL-6	Interleukin-6
Arg-1	Arginase-1
iNOS	inducible Nitric Oxide Synthase
H & E	Hematoxylin and Eosin
BCA	Bicinchoninic Acid
BALF	Bronchoalveolar Lavage Fluid

Acknowledgements
This work was supported by National Natural Science Foundation of China (82374266, 81973670), Key Projects of Traditional Chinese Medicine Research in Hunan Province (A2024010), Excellent Youth Project of Hunan Provincial Department of Education (23B0379), Natural Science Foundation of Hunan Province (2023JJ10031), Outstanding Innovative Youth Project of Changsha (kq2209019), National College Student Innovation and Entrepreneurship Training Program (S202410541014).

Author contributions
L.L.,F.L. and Y.N. conceived the experiments, and supervised the study. J.F., Z.L.,Z.F. performed the experiments, analyzed the data, and prepared the manuscript. J.H.,J.S.and K.W. provided experimental materials and insightful suggestions. X.J. and J.Y. wrote and revised the manuscript. All authors read and approved the final manuscript.

Data availability
No datasets were generated or analysed during the current study.

Declarations

Ethics approval and consent to participate
All animal experiments were approved by the Ethics Committee of the Center for Animal Experiments of Hunan University of Chinese Medicine (Approval number: SLBH-202307190001).

Consent for publication
All authors have approved the manuscript and agree with the submission.

Competing interests
The authors declare no competing interests.

Author details
[1]College of Traditional Chinese Medicine, Hunan University of Chinese Medicine, Xueshi 300 Road, Changsha, Hunan 410208, PR China
[2]College of Integrated Traditional Chinese and Western Medicine, Hunan University of Chinese Medicine, Xueshi Road 300, Changsha, Hunan 410208, PR China
[3]The Medicine School, Hunan University of Chinese Medicine, Xueshi Road 300, Changsha, Hunan 410208, PR China
[4]Hunan Provincial Key Laboratory of Integrated Traditional Chinese and Western Medicine, Hunan University Of Chinese Medicine, Xueshi Road 300, Changsha, Hunan 410208, PR China

Received: 7 October 2024 / Accepted: 14 March 2025
Published online: 04 April 2025

References

1. Zhang J, Guo Y, Mak M, Tao Z. Translational medicine for acute lung injury. J Transl Med. 2024;22(1):25.
2. Liu C, Xiao K, Xie L. Advances in the use of exosomes for the treatment of ALI/ARDS. Front Immunol. 2022;13:971189.
3. Meng J, Leung KS, Jiang Z, Dong X, Zhao Z. Establishment of GC-MS fingerprint of fresh houttuynia cordata. Chem Pharm Bull (Tokyo). 2005;53(11):1484–9.
4. Zheng Y, Lei L, Liang S, et al. Protective effect of fresh/dry dandelion extracts on APAP-Overdose-Induced acute liver injury. Chin J Integr Med. 2022;28(8):683–92.
5. Zhang L, Wang Y, Yang D, et al. Platycodon grandiflorus - an ethnopharmacological, phytochemical and Pharmacological review. J Ethnopharmacol. 2015;164:147–61.
6. Liu Y, Dong Y, Shen W, et al. Platycodon grandiflorus polysaccharide regulates colonic immunity through mesenteric lymphatic circulation to attenuate ulcerative colitis. Chin J Nat Med. 2023;21(4):263–78.
7. Xu M, Qi Y, Liu G, Song Y, Jiang X, Du B. Size-Dependent in vivo transport of nanoparticles: implications for delivery, targeting, and clearance. ACS Nano. 2023;17(21):20825–49.
8. Ye QN, Zhu L, Liang J, et al. Orchestrating NK and T cells via tri-specific nano-antibodies for synergistic antitumor immunity. Nat Commun. 2024;15(1):6211.
9. Shu Z, Zhang C, Yan L, et al. Antibacterial and osteoconductive Polycaprolactone/polylactic acid/nano-hydroxyapatite/Cu@ZIF-8 GBR membrane with asymmetric porous structure. Int J Biol Macromol. 2023;224:1040–51.
10. Tu C, Lu H, Zhou T, et al. Promoting the healing of infected diabetic wound by an anti-bacterial and nano-enzyme-containing hydrogel with inflammation-suppressing, ROS-scavenging, oxygen and nitric oxide-generating properties. Biomaterials. 2022;286:121597.
11. Lv Y, Li W, Liao W, et al. Nano-Drug delivery systems based on natural products. Int J Nanomed. 2024;19:541–69.
12. Huang L, Huang XH, Yang X, et al. Novel nano-drug delivery system for natural products and their application. Pharmacol Res. 2024;201:107100.
13. Barzin M, Bagheri AM, Ohadi M, Abhaji AM, Salarpour S, Dehghannoudeh G. Application of plant-derived exosome-like nanoparticles in drug delivery. Pharm Dev Technol. 2023;28(5):383–402.
14. Chu K, Liu J, Zhang X, et al. Herbal Medicine-Derived Exosome-Like nanovesicles: A rising star in cancer therapy. Int J Nanomed. 2024;19:7585–603.
15. Kim J, Zhang S, Zhu Y, Wang R, Wang J. Amelioration of colitis progression by ginseng-derived exosome-like nanoparticles through suppression of inflammatory cytokines. J Ginseng Res. 2023;47(5):627–37.
16. Zhang X, Pan Z, Wang Y, Liu P, Hu K. Taraxacum officinale-derived exosome-like nanovesicles modulate gut metabolites to prevent intermittent hypoxia-induced hypertension. Biomed Pharmacother. 2023;161:114572.
17. Zhang W, Song Q, Bi X, et al. Preparation of pueraria Lobata Root-Derived Exosome-Like nanovesicles and evaluation of their effects on mitigating alcoholic intoxication and promoting alcohol metabolism in mice. Int J Nanomed. 2024;19:4907–21.
18. Yao Z. A study on the evaluation of the superior efficacy of fresh use of traditional Chinese medicine: a case study of dandelion. MA thesis. South-Central University for Nationalities; 2021, https://doi.org/10.27710/d.cnki.gznmc.2020.000403
19. Xia L, Zhang C, Lv N, et al. AdMSC-derived exosomes alleviate acute lung injury via transferring mitochondrial component to improve homeostasis of alveolar macrophages. Theranostics. 2022;12(6):2928–47.
20. Ochando J, Mulder W, Madsen JC, Netea MG, Duivenvoorden R. Trained immunity - basic concepts and contributions to immunopathology. Nat Rev Nephrol. 2023;19(1):23–37.
21. Liang D, Liu C, Yang M. Mesenchymal stem cells and their derived exosomes for ALI/ARDS: A promising therapy. Heliyon. 2023;9(10):e20387.

22. Zhang S, Chai X, Hou G, Zhao F, Meng Q. Platycodon grandiflorum (Jacq.) A. DC.: A review of phytochemistry, pharmacology, toxicology and traditional use. Phytomedicine. 2022;106:154422.
23. Ren H, Peng D, Liu M, et al. Dynamic changes in chemical components, volatile profile and antioxidant properties of Xanthoceras sorbifolium leaf tea during manufacturing process. Food Chem. 2025;468:142409.
24. Feng J, Xiu Q, Huang Y, Troyer Z, Li B, Zheng L. Plant-Derived Vesicle-Like nanoparticles as promising biotherapeutic tools: present and future. Adv Mater. 2023;35(24):e2207826.
25. Karamanidou T, Tsouknidas A. Plant-Derived extracellular vesicles as therapeutic nanocarriers. Int J Mol Sci. 2021;23(1):191.
26. Lian MQ, Chng WH, Liang J, et al. Plant-derived extracellular vesicles: recent advancements and current challenges on their use for biomedical applications. J Extracell Vesicles. 2022;11(12):e12283.
27. Zhu MZ, Xu HM, Liang YJ, et al. Edible exosome-like nanoparticles from portulaca Oleracea L mitigate DSS-induced colitis via facilitating double-positive CD4(+)CD8(+)T cells expansion. J Nanobiotechnol. 2023;21(1):309.
28. Hwang JH, Park YS, Kim HS, et al. Yam-derived exosome-like nanovesicles stimulate osteoblast formation and prevent osteoporosis in mice. J Control Release. 2023;355:184–98.
29. Shapouri-Moghaddam A, Mohammadian S, Vazini H, et al. Macrophage plasticity, polarization, and function in health and disease. J Cell Physiol. 2018;233(9):6425–40.
30. Mosser DM, Hamidzadeh K, Goncalves R. Macrophages and the maintenance of homeostasis. Cell Mol Immunol. 2021;18(3):579–87.
31. Ross EA, Devitt A, Johnson JR, Macrophages. The good, the bad, and the gluttony. Front Immunol. 2021;12:708186.
32. Zhang M, Li X, Zhang Q, Yang J, Liu G. Roles of macrophages on ulcerative colitis and colitis-associated colorectal cancer. Front Immunol. 2023;14:1103617.
33. Liu T, Wang L, Liang P, et al. USP19 suppresses inflammation and promotes M2-like macrophage polarization by manipulating NLRP3 function via autophagy. Cell Mol Immunol. 2021;18(10):2431–42.
34. Faas M, Ipseiz N, Ackermann J, et al. IL-33-induced metabolic reprogramming controls the differentiation of alternatively activated macrophages and the resolution of inflammation. Immunity. 2021;54(11):2531–e25465.
35. Shen L, Li H, Chen W, et al. Integrated application of transcriptome and metabolomics reveals potential therapeutic targets for the polarization of atherosclerotic macrophages. Biochim Biophys Acta Mol Basis Dis. 2022;1868(12):166550.
36. Jin J, Gao L, Zou X, et al. Gut dysbiosis promotes preeclampsia by regulating macrophages and trophoblasts. Circ Res. 2022;131(6):492–506.
37. Palmieri EM, Gonzalez-Cotto M, Baseler WA, et al. Nitric oxide orchestrates metabolic rewiring in M1 macrophages by targeting aconitase 2 and pyruvate dehydrogenase. Nat Commun. 2020;11(1):698.
38. Vassiliou E, Farias-Pereira R. Impact of lipid metabolism on macrophage polarization: implications for inflammation and tumor immunity. Int J Mol Sci. 2023;24(15):12032.
39. Yan J, Horng T. Lipid metabolism in regulation of macrophage functions. Trends Cell Biol. 2020;30(12):979–89.
40. Liu LW, Shi YY, Li ZL, et al. Metabolomic insights into the synergistic effect of Biapenem in combination with Xuebijing injection against sepsis. Front Pharmacol. 2020;11:502.
41. Neugebauer S, Giamarellos-Bourboulis EJ, Pelekanou A, et al. Metabolite profiles in sepsis: developing prognostic tools based on the type of infection. Crit Care Med. 2016;44(9):1649–62.
42. Judd JM, Jasbi P, Winslow W, et al. Inflammation and the pathological progression of Alzheimer's disease are associated with low Circulating choline levels. Acta Neuropathol. 2023;146(4):565–83.
43. Sanchez-Lopez E, Zhong Z, Stubelius A, et al. Choline uptake and metabolism modulate macrophage IL-1β and IL-18 production. Cell Metab. 2019;29(6):1350–e13627.
44. Luo S, Lin H, Wu C, et al. Cholinergic macrophages promote the resolution of peritoneal inflammation. Proc Natl Acad Sci U S A. 2024;121(27):e2402143121.
45. Liu Y, Xu R, Gu H, et al. Metabolic reprogramming in macrophage responses. Biomark Res. 2021;9(1):1.
46. Cao J, Zeng F, Liao S, Cao L, Zhou Y. Effects of Glycolysis on the polarization and function of tumor–associated macrophages (Review). Int J Oncol. 2023;62(6):70. [pii].
47. Ye L, Jiang Y, Zhang M. Crosstalk between glucose metabolism, lactate production and immune response modulation. Cytokine Growth Factor Rev. 2022;68:81–92.
48. Chandel NS, Glycolysis. Cold Spring Harb Perspect Biol. 2021;13(5):a040535.
49. Hwang JS, Kim KH, Park J, et al. Glucosamine improves survival in a mouse model of sepsis and attenuates sepsis-induced lung injury and inflammation. J Biol Chem. 2019;294(2):608–22.

Publisher's note